Research Square

Preprints are preliminary reports that have not undergone peer review.
They should not be considered conclusive, used to inform clinical practice,
or referenced by the media as validated information.

The wheat Lr28 locus harbors three tandem NLR genes that independently confer leaf rust resistance

Shisheng Chen

shisheng.chen@pku-iaas.edu.cn

Peking University Institute of Advanced Agricultural Sciences, Shandong Laboratory of Advanced Agriculture Sciences in Weifang https://orcid.org/0000-0002-8617-4356

Liang Qiao

Peking University Institute of Advanced Agricultural Sciences, Shandong Laboratory of Advanced Agriculture Sciences in Weifang

Hongna Li

State Key Laboratory of Wheat Improvement, Peking University Institute of Advanced Agricultural Sciences, Shandong Laboratory of Advanced Agriculture Sciences in Weifang https://orcid.org/0000-0002-8994-2664

Rui Song

Peking University Institute of Advanced Agricultural Sciences, Shandong Laboratory of Advanced Agriculture Sciences in Weifang https://orcid.org/0009-0001-9762-8093

Qing Wang

Peking University Institute of Advanced Agricultural Sciences, Shandong Laboratory of Advanced Agriculture Sciences in Weifang

Shams ur Rehman

State Key Laboratory of Wheat Improvement, Peking University Institute of Advanced Agricultural Sciences, Shandong Laboratory of Advanced Agriculture Sciences in Weifang, Shandong 261325, China

Ming Hao

Sichuan Agricultural University https://orcid.org/0000-0003-2693-3864

Xiaodong Wang

Hebei Agricultural University https://orcid.org/0000-0002-4304-5482

Haitao Yu

Peking University Institute of Advanced Agricultural Sciences, Shandong Laboratory of Advanced Agriculture Sciences in Weifang

Yi Ding

The University of Sydney https://orcid.org/0000-0002-1356-4863

Peng Zhang

University of Sydney https://orcid.org/0000-0002-4191-1068

Article

Keywords: Lr28, Aegilops speltoides, wheat, leaf rust, CC-NBS-LRR, genome assembly

Posted Date: November 6th, 2026

DOI: https://doi.org/10.21203/rs.3.rs-11240051/v1

License: This work is licensed under a Creative Commons Attribution 4.0 International License.
Read Full License

Additional Declarations: Yes there is potential Competing Interest. S.C., H.L., L.Q., R.S., and S.u.R. are inventors on a Chinese provisional patent application (China patent filing No. 202611271684.8) relating to the use of the Lr28 gene in wheat breeding programs.

The wheat *Lr28* locus harbors three tandem NLR genes that independently confer leaf rust resistance

Liang Qiao[1#], Hongna Li[1#], Rui Song[1#], Qing Wang[1#], Shams ur Rehman[1], Ming Hao[2], Xiaodong Wang[3], Haitao Yu[1], Yi Ding[4], Peng Zhang[4], Shisheng Chen[1*]

[1]State Key Laboratory of Wheat Improvement, Peking University Institute of Advanced Agricultural Sciences, Shandong Laboratory of Advanced Agriculture Sciences in Weifang, Shandong 261325, China

[2]State Key Laboratory of Crop Gene Exploration and Utilization in Southwest China, Sichuan Agricultural University, Chengdu 611130, Sichuan, China

[3]State Key Laboratory of North China Crop Improvement and Regulation, College of Plant Protection, Hebei Agricultural University, Baoding, Hebei 071000, China

[4]School of Life and Environmental Sciences, Faculty of Science, The University of Sydney, Sydney, NSW 2570, Australia

#These authors contributed equally: Liang Qiao, Hongna Li, Rui Song, Qing Wang

*Corresponding author: S. Chen, Email address: shisheng.chen@pku-iaas.edu.cn

Shisheng Chen https://orcid.org/0000-0002-8617-4356
Liang Qiao https://orcid.org/0000-0002-0600-3478
Hongna Li https://orcid.org/ 0000-0002-8994-2664
Rui Song https://orcid.org/0009-0001-9762-8093

ABSTRACT

Leaf rust is a devastating wheat disease, and deploying resistant cultivars is the most effective control strategy. Here, we report a high-quality genome assembly for the *Lr28* introgression line GSTR 428 and use this resource to clone *Lr28*, a resistance locus introgressed from an *Aegilops speltoides* segment into wheat chromosome arm 4AL. The *Lr28* locus comprises three tandem NLR genes (*CNL1*-*CNL3*), each of which is independently sufficient to confer resistance, as demonstrated by CRISPR/Cas9-induced mutations and transgenic complementation. CNL1 and CNL2 are identical and share 99.03% protein sequence identity with CNL3. The same three genes occur in four *Ae. speltoides* accessions. We further demonstrate that *Lr28* underlies the major 4AL resistance QTL identified by genome-wide association study (GWAS) in European wheat cultivars. To reduce linkage drag, we generate shortened alien segments (<1.22 Mb) harboring *Lr28* using the *ph1b* mutant. The cloning of *Lr28* will accelerate its deployment in wheat breeding programs.

Keywords: *Lr28*, *Aegilops speltoides*, wheat, leaf rust, CC-NBS-LRR, genome assembly

INTRODUCTION

Wheat (*Triticum aestivum* L., AABBDD) is a major crop that feeds billions of people worldwide. With the global human population projected to reach 9.7 billion by 2050, wheat production must increase by more than 50% to meet rising food demand[1]. Achieving this goal requires the development of elite wheat cultivars with improved resistance to biotic and abiotic stress factors. Among biotic threats, rust diseases caused by fungal pathogens are particularly devastating. Leaf rust, caused by *Puccinia triticina* (*Pt*), is one of the most widespread and destructive foliar diseases of wheat. Severe epidemics can reduce yields by over 50%, posing a major threat to global food security[2,3]. Although chemical fungicides can control rust, their high cost, potential health risks, and environmental concerns limit their widespread use. Therefore, breeding wheat varieties with effective resistance genes remains the most economical, environmentally friendly, and sustainable strategy[4].

To date, more than 80 leaf rust resistance (*Lr*) genes derived from wheat or its wild relatives have been officially designated[5,6]. However, owing to the complexity of the wheat genome, only 14 *Lr* genes have been cloned[7]. These include two slow-rusting, multi-pathogen resistance genes (*Lr34/Yr18/Sr57/Pm38* and *Lr67/Yr46/Sr55/Pm46*)[8,9] and 12 race-specific resistance genes (*Lr1*[10], *Lr9*/*Lr58*[11], *Lr10*[12], *Lr13*[13,14], *Lr14a*[15], *Lr21*[16], *Lr22a*[17], *Lr30/Lr.ace-4A*[7], *Lr39/Lr41*[18,19], *Lr42*[20], *Lr47*[21], and *Lr85*[6]). The resistance genes *Lr34* and *Lr67* encode an ATP-binding cassette transporter and a hexose transporter, respectively[8,9]. *Lr9*/*Lr58* and *Lr39/Lr41* encode proteins with tandem kinase domains[11,18,19]. *Lr14a* encodes a membrane-localized protein containing 12 ankyrin repeats[15]. *Lr30*/*Lr.ace-4A* encodes a non-canonical coiled-coil nucleotide-binding leucine-rich repeat (NLR) receptor with tandem nucleotide-binding domains[7]. The remaining cloned *Lr* genes encode typical NLR proteins[6,7,21].

Most isolated resistance genes in wheat encode intracellular NLR proteins[22], which detect specific pathogen effectors and activate immune responses. In most cases, a single resistance locus harbors one NLR protein[21,23-25]. However, accumulating evidence shows that NLRs often function cooperatively as “sensor-helper” pairs. In wheat, several such paired NLRs have been identified, including *TdCNL1*/*TdCNL5*,

TdNLR1/*TdNLR2*, *CNL*/*NL*, $Yr6^{RL}$/$Yr6^{CNL1}$, and *RXL*/*Pm5e*[26-30]. Moreover, three studies have shown that complementary NLR pairs (*MlIW39-R1*/*R2*, *Pm68-1*/*2*, and *PmWR183-NLR1*/*NLR2*) coordinately confer powdery mildew resistance[31-33]. These findings highlight the complexity of NLR gene clusters in conferring disease resistance.

The continuous evolution of new *Pt* races has made many *Lr* genes ineffective[34,35]. Therefore, cloning additional *Lr* genes is essential to diversify the resistance sources available for gene pyramids or transgenic cassettes. The diploid wheat relative *Aegilops speltoides* (2n = 2x = 14, SS), the closest known donor of the B subgenome to bread wheat[36,37], represents an invaluable reservoir of *Lr* genes[21]. Several genes, including *Lr28*, *Lr35*, *Lr36*, *Lr47*, *Lr51*, and *Lr66*, have been successfully introgressed from *Ae. speltoides* into common wheat[38]. Among these, *Lr28* was introduced into bread wheat by Riley et al. (1968) during their efforts to transfer *Yr8*[39]. The introgressed segment originated from the short arm of chromosome 7S and was incorporated into chromosome arm 4AL[40]. This alien segment was subsequently backcrossed into different wheat genetic backgrounds in India and Australia[41,42]. It was also transferred into the "Thatcher" background, which is widely used for developing near-isogenic lines (NILs) for leaf rust resistance studies[43]. Although virulence against *Lr28* has been reported in India[44], Australia[4], and Europe[45], its frequency remains very low. This gene still confers significant resistance across many wheat-growing regions, with particularly high efficacy in Asia[46-49], and may play a key role in improving wheat resistance to leaf rust.

Here, we generated a high-quality genome assembly (contig N50 = 101.48 Mb) of the *Lr28* introgression line GSTR 428 and successfully isolated the resistance genes. The *Lr28* locus contains three tandem NLR genes (*CNL1*-*CNL3*), each independently capable of conferring leaf rust resistance. CNL1 and CNL2 are 100% identical and share 99.03% protein sequence identity with CNL3. We further demonstrate that *Lr28* is the causal gene underlying the major 4AL GWAS resistance locus in European wheat. To enhance breeding utility, we used the *ph1b* mutant to minimize the introgressed segment to <1.22 Mb and developed diagnostic markers for marker-assisted selection.

RESULTS

Characterization of leaf rust resistance in GSTR 428

The introgression line GSTR 428 (Thatcher*6/*Aegilops speltoides*) is near-isogenic to the wheat variety Thatcher and carries the introgressed *Ae. speltoides* segment 7S#2. In seedling tests, GSTR 428 exhibited near-immunity to all ten Chinese *Pt* pathotypes tested (Supplementary Table 1), whereas the recurrent parent Thatcher was highly susceptible, displaying infection types (ITs) ranging from 3 to 4 (Fig. 1a).

Following inoculation with *Pt* pathotype PHQS, Thatcher developed abundant rust pustules with visible sporulation from 6 days post-inoculation (dpi) onward, whereas GSTR 428 exhibited a hypersensitive response with no visible spore production (Supplementary Fig. 1a). Microscopic examination using WGA-FITC staining revealed that fungal hyphae were effectively confined in GSTR 428, while in Thatcher the pathogen formed an extensive and diffuse mycelial network (Supplementary Fig. 1b). Quantitative assessments across 2, 4, 6, and 8 dpi confirmed that the infection foci in GSTR 428 were significantly smaller than those in Thatcher ($P < 0.01$, Supplementary Fig. 1c).

All F_1 progeny derived from the cross between GSTR 428 and the Chinese Spring *ph1b* mutant (CS*ph1b*) displayed resistance (ITs = 0;) to *Pt* pathotype PHQS. Phenotypic evaluation of 122 F_2 individuals revealed 99 resistant and 23 susceptible plants (Supplementary Fig. 2). This distribution did not deviate significantly from the expected 3:1 segregation ratio for a single dominant gene ($\chi^2 = 2.46$, $P = 0.12$).

Characterization of the alien segment carrying *Lr28*

To characterize the alien segment in GSTR 428, we performed read-depth (coverage) analysis. Alignment of GSTR 428 whole-genome resequencing reads to the Chinese Spring (CS) reference genome (CS-IAAS[50]) identified a region with significantly reduced coverage extending from ~726.90 Mb to the distal end of chromosome arm 4AL (Supplementary Fig. 3), indicating an alien segment of ~41.42 Mb based on the CS-IAAS assembly. This alien translocation was further validated by genomic *in situ* hybridization (GISH) and fluorescence *in situ* hybridization (FISH), which confirmed

its presence at the telomeric region of chromosome arm 4AL in GSTR 428 (Fig. 1b).

High-quality genome assembly and annotation of GSTR 428

Since *Lr28* originates from a complex translocation involving chromosomes 7S and 4A, we generated a chromosome-scale reference genome for the introgression line GSTR 428 to facilitate cloning of this resistance locus. Using 729.57 Gb of PacBio High-Fidelity (HiFi) reads and 1199.55 Gb of high-throughput chromosome conformation capture sequencing (Hi-C) reads (Supplementary Table 2), we assembled a 14.47-Gb genome, with 14.43 Gb (99.72%) anchored to 21 chromosomes and a contig N50 of 101.48 Mb (Fig. 1c; Supplementary Fig. 4 and Supplementary Table 3). The assembly quality was validated by an LTR Assembly Index (LAI) score of 17.91, a Quality value (QV) score of 58.89, and a Benchmarking Universal Single-Copy Orthologs (BUSCO) completeness score of 99.08%, reflecting high contiguity and completeness (Supplementary Table 3). Additionally, the raw HiFi reads mapped to the assembly at an overall rate of 99.65% and exhibited uniform coverage across all chromosomes (Supplementary Fig. 5). Similarly, the Hi-C reads achieved a mapping rate of 99.92%.

Using a combination of homoeologous protein sequences, Iso-Seq data, and RNA-seq data collected from four tissues (leaf, root, stem, and spike) at both seedling and adult stages, we predicted 126,929 high-confidence genes in the GSTR 428 genome (Supplementary Tables 2 and 3). Repetitive sequences account for 12.21 Gb (84.37%) of the genome, dominated by Gypsy (45.54%) and Copia (16.37%) long terminal repeat retrotransposons. Whole-genome sequence alignment revealed largely conserved collinearity between GSTR 428 and the CS-IAAS reference genome (Supplementary Fig. 6). Nevertheless, we identified 35,180 structural variants (SVs), including 219 large SVs (>50 kb) (Fig. 1d; Supplementary Table 4). Notably, the distal end of chromosome arm 4AL, which carries a well-documented 4AL/7BS reciprocal translocation arising during wheat polyploidization[51], exhibited clear collinearity disruptions between the two assemblies (Fig. 1d). Synteny analysis based on high-confidence genes demonstrated that the alien 7S#2 segment in GSTR 428 was introgressed from the distal short arm of chromosome 7S (Fig. 1e). To precisely define

the translocation breakpoint, we analyzed read depth and variant distribution using Thatcher resequencing reads aligned to the GSTR 428 genome, and identified a clear breakpoint at ~712.80 Mb in GSTR 428 (Fig. 1f). The introgressed alien segment spans ~46.45 Mb in the GSTR 428 assembly.

Genetic mapping of *Lr28* using the GSTR 428 genome

To induce recombination between the introgressed 7S#2 segment and the homoeologous 7BS region (which is involved in the 4AL/7BS reciprocal translocation), we constructed the GSTR 428 × CS*ph1b* mapping population. Twelve F_2 plants heterozygous for the alien 7S segment and homozygous for *ph1b* were self-pollinated to produce F_3 seeds for recombination screening. Initial mapping using 408 plants from segregating F_3 families and eight cleaved amplified polymorphic sequence (CAPS) markers distributed across the introgressed *Ae. speltoides* segment (Supplementary Table 5) placed *Lr28* between markers *pku600* and *pku863* (Fig. 2a). To refine the interval, we genotyped an additional 1,121 F_3 plants and screened for recombinants between markers *pku600* and *pku863*. Seven distinct *Ae. speltoides* segment lengths were identified and designated L1 to L7 (Fig. 2a). Using these recombinants and six newly developed markers (Supplementary Table 5), we further delimited *Lr28* to a 1.22-Mb region flanked by markers *pku697* and *pku095*, with *pku715* showing complete linkage to *Lr28* (Fig. 2a). This candidate region contains 31 high-confidence genes (*GSTR428.4A01G00525300-GSTR428.4A01G00528300*), including four typical NLR genes (Supplementary Table 6). Sequence analysis revealed that three of them are intact NLR genes (designated *CNL1*, *CNL2*, and *CNL3*), whereas the fourth carries premature stop codons and is thus a truncated NLR gene (designated *cnl4*). The physical distance between *CNL1* and *CNL2* is 24.83 kb, and that between *CNL2* and *CNL3* is 24.68 kb (GSTR 428 coordinates; Supplementary Table 6). All three genes are located on the negative strand and share the same transcriptional orientation.

To assess collinearity, we compared the GSTR 428 candidate interval against the genomes of three *Ae. speltoides* accessions (AEG-9674-1, Y2032, and TS01)[52-54] and the wheat reference CS-IAAS[50]. Relative to CS-IAAS, the interval in GSTR 428 exhibited marked sequence deletions and rearrangements, accompanied by a

considerable reduction in physical size (Fig. 2b). Compared with the three *Ae. speltoides* accessions, GSTR 428 also displayed extensive sequence variation and structural rearrangements within the candidate interval (Fig. 2b).

Candidate gene identification for *Lr28* via EMS mutagenesis and transcriptomics

EMS mutagenesis of GSTR 428 generated 886 independent M_2 mutant families. Phenotypic screening with *Pt* pathotype PHQS identified only two mutants (M56 and M473) showing susceptible plants (Fig. 2c). Genotyping with 14 genome-specific markers revealed that both mutants retained only truncated portions of the introgressed 7S segment (Supplementary Table 7). Consistently, read-depth analysis based on whole-genome resequencing identified a 6.60-Mb deletion in M56 (spanning 739.95-746.55 Mb) and a larger deletion in M473 extending from 721.45 Mb to the distal end of chromosome 4AL (Fig. 2d). The deleted regions in both mutants overlapped with the mapped interval, confirming the genetic mapping results.

Transcript levels of the candidate genes were examined using RNA-seq data from GSTR 428 and Thatcher at 72 hours post-inoculation (hpi) with PHQS. Among the 31 annotated genes within the candidate region, 13 exhibited significantly higher expression in GSTR 428 than in Thatcher (FDR < 0.05, *p*-value < 0.05, $|\log_2 \text{foldchange}| > 1$; Supplementary Table 8). These included *CNL1*, *CNL2*, and *CNL3* (*GSTR428.4A01G00526700-GSTR428.4A01G00526900*; Supplementary Fig. 7), which were expressed in GSTR 428 but were either absent or not expressed in Thatcher (Fig. 2e). All three genes are intron-free and encode NLR proteins of 1,239 amino acids (GenBank accession numbers PZ791522, PZ791523, and PZ791524), with their LRR domain comprising two discontinuous blocks (Fig. 2f). Sequence alignment revealed that the coding sequence (CDS) of *CNL1* is identical to that of *CNL2*, encoding the same protein. By contrast, CNL3 differs from CNL1/CNL2 by 12 amino acid residues, corresponding to 99.03% protein sequence identity (Fig. 2f). Polymorphisms in the 3′-untranslated region (UTR) and coding sequences enabled the design of gene-specific primers (Supplementary Fig. 8), which confirmed the presence of all three genes by PCR and Sanger sequencing. AlphaFold-predicted structures of the full-length proteins revealed high architectural conservation between CNL1/CNL2 and CNL3

(Supplementary Fig. 9). Collectively, *CNL1*, *CNL2*, and *CNL3* were identified as the candidate genes for *Lr28*.

CRISPR/Cas9-mediated functional validation of candidate genes

To functionally validate the candidate genes, we established a CRISPR/Cas9-based gene editing system in GSTR 428, incorporating Cas9-Trex2 and GRF4-GIF1 fusion proteins to enhance editing and regeneration efficiency[55,56]. A guide RNA (gRNA) was designed to simultaneously target *CNL1*, *CNL2*, and *CNL3* (5′-TTATGTGTGTGACTCTCGAA-3′; Fig. 3a). Gene-specific primers covering the gRNA region were designed based on polymorphisms in the coding and 3′ UTR sequences (Supplementary Fig. 8). From 70 independent transgenic T_0 plants, 65 (92.86%) were confirmed to carry mutations at the target sites. Among these, two T_0 plants (T_0KO-1 and T_0KO-2) harbored homozygous loss-of-function mutations in all three *CNL* genes simultaneously (Fig. 3a). Phenotypic evaluation of these T_0 plants and their T_1 progeny revealed that plants carrying homozygous mutations in all three *CNL* genes were fully susceptible to *Pt* pathotype PHQS (Fig. 3b, c).

In addition, three T_1 plants (T_1KO-3, T_1KO-4, and T_1KO-5) were identified, each carrying homozygous loss-of-function mutations in two of the three genes, with the remaining gene unedited (Fig. 3a). These plants, together with their T_2 progeny that retained the same editing configuration as confirmed by Sanger sequencing, maintained robust resistance to PHQS (Fig. 3c and Supplementary Fig. 10). Collectively, these results demonstrate that any single *CNL* gene is sufficient to confer resistance; the three genes function redundantly against PHQS, and only their simultaneous disruption abolishes resistance.

Transgenic overexpression and complementation validate the candidate genes

We constructed two overexpression vectors: one carrying *CNL1*/*CNL2* (which share identical CDS) and the other carrying *CNL3*, with expression driven by the maize *ubiquitin* (Ubi) promoter (Fig. 3d, e). Each construct was introduced separately into the spring wheat cultivar Fielder via *Agrobacterium tumefaciens*-mediated transformation. We generated 32 independent T_0 transgenic plants for pUbi::*CNL1*/*CNL2* (C721) and 28 T_0 plants for pUbi::*CNL3* (C722), from which eight

positive T_0 plants per construct were randomly selected for detailed analysis. Transgene presence and expression were confirmed by PCR and qRT-PCR (Supplementary Figs. 11 and 12; Supplementary Table 9). Upon inoculation with *Pt* pathotype PHQS, both T_0 and T_1 transgenic plants overexpressing either *CNL1*/*CNL2* or *CNL3* exhibited robust resistance, whereas the Fielder control displayed complete susceptibility (Fig. 3f, g; Supplementary Figs. 11d and 12d).

We further introduced the genomic fragments of *CNL1* (8,056 bp) and *CNL3* (8,233 bp), each including its native regulatory sequences, into Fielder in separate transformation experiments (Fig. 3h, i). A total of 20 and 22 independent T_0 plants were generated for *CNL1* (C734) and *CNL3* (C749), respectively, and eight from each construct were randomly selected for further analysis. PCR and qRT-PCR confirmed transgene presence and expression in the selected plants (Supplementary Figs. 13 and 14; Supplementary Table 10). When challenged with PHQS, all T_0 and T_1 plants expressing either *CNL1* or *CNL3* alone exhibited robust resistance, whereas Fielder remained highly susceptible (Fig. 3j, k; Supplementary Figs. 13d and 14d). These results demonstrate that transgenic expression of any single *CNL* gene is sufficient to confer resistance to leaf rust.

Taken together, the genetic mapping, CRISPR/Cas9-induced mutagenesis, and transgenic complementation/overexpression experiments demonstrate that the *Lr28* locus comprises three tandem NLR genes, each capable of independently conferring resistance against the tested pathotype PHQS. These genes are hereafter designated $Lr28^{CNL1}$, $Lr28^{CNL2}$, and $Lr28^{CNL3}$.

$Lr28^{CNL1/CNL2}$ and $Lr28^{CNL3}$ confer identical resistance profiles

$Lr28^{CNL1/CNL2}$ and $Lr28^{CNL3}$ share 99.03% protein sequence identity, with 12 amino acid substitutions between them, which might suggest distinct recognition specificities. To investigate this, two independent T_1 overexpression lines for $Lr28^{CNL1/CNL2}$ (T_1C721-6 and T_1C721-8) and two for $Lr28^{CNL3}$ (T_1C722-1 and T_1C722-5) were inoculated with seven *Pt* pathotypes virulent to Fielder. All transgenic lines overexpressing either $Lr28^{CNL1/CNL2}$ or $Lr28^{CNL3}$ exhibited robust resistance to all pathotypes tested (Fig. 4a). These results demonstrate that, among the pathotypes examined, $Lr28^{CNL1/CNL2}$ and

$Lr28^{CNL3}$ confer identical resistance profiles.

Haplotype analysis and diagnostic marker of *Lr28*

A BLASTP search against the published genomes of *Aegilops*, *Triticum*, and other Triticeae species, together with the NCBI non-redundant protein database, revealed that the closest homologs of $Lr28^{CNL1/CNL2}$ and $Lr28^{CNL3}$ share less than 87.16% amino acid identity (Supplementary Fig. 15). To examine the relationships between these proteins and other known resistance (R) proteins in Poaceae, we performed a phylogenetic analysis including $Lr28^{CNL1/CNL2}$, $Lr28^{CNL3}$ and 207 previously cloned R proteins. The resulting tree placed the Lr28 proteins in the same clade as RDG2A, a barley leaf stripe resistance protein (Supplementary Fig. 16), with which they share ~79.1% sequence similarity. Most of the sequence variation between the Lr28 proteins and RDG2A was concentrated in the LRR domain.

To further investigate sequence variation at this locus, we amplified and Sanger-sequenced the coding regions of $Lr28^{CNL1}$, $Lr28^{CNL2}$, and $Lr28^{CNL3}$ from 94 *Ae. speltoides* accessions (Supplementary Table 11) using gene-specific primers. Among these, four accessions (T2140003, T2140004, PI 369596, and PI 542268) carried the complete set of all three genes, with sequences 100% identical to those in GSTR 428. Three accessions (PI 369590, PI 369591, and PI 369604) harbored $Lr28^{CNL2}$ but lacked both $Lr28^{CNL1}$ and $Lr28^{CNL3}$. All seven accessions in these two groups exhibited near-immunity to PHQS. Seven additional accessions (PI 486263, PI 554297, PI 554303, PI 554295, PI 542266, PI 573450, and PI 573452) carried only a single gene highly similar to either $Lr28^{CNL1/CNL2}$ or $Lr28^{CNL3}$, with two to four additional amino acid differences (Fig. 4b). All seven variant-carrying accessions were also resistant to PHQS (Supplementary Table 12); however, whether this resistance is mediated by the *Lr28* locus or by other resistance genes remains to be determined.

A dominant marker, *Lr28MASF1R1* (Supplementary Table 5), was developed based on a critical cDNA polymorphism, 2977-2978TG (amino acid 993C), which distinguishes the Lr28 proteins from all known homologs in published Triticeae genomes (Supplementary Fig. 17). Marker screening of 87 *T. turgidum* and 151 *T. aestivum* accessions revealed that, apart from GSTR 428, none produced the expected

PCR amplicon, indicating the absence of *Lr28* in these genotypes (Supplementary Table 13). This marker was also used to evaluate the 94 *Ae. speltoides* accessions described above, and only the 14 previously identified accessions yielded the expected amplicon (Supplementary Fig. 18; Supplementary Table 13).

_Lr28_ underlies the major 4AL leaf rust resistance QTL

Previous GWAS mapped a major leaf rust resistance locus to the distal end of chromosome arm 4AL[57,58]. The GWAS peak overlaps a 26-Mb interval of pronounced sequence divergence between the winter wheat cultivar Attraktion and CS, indicative of an alien introgression inferred to originate from *T. dicoccoides*[58,59]. BLAST analysis against the publicly available Attraktion genome assembly revealed that Attraktion harbors all three *Lr28* genes with 100% sequence identity to the GSTR 428 alleles, confirming that the *Lr28* locus is responsible for the strong resistance in this cultivar. The same introgressed segment has also been postulated to be present in 13 other wheat cultivars (KWS Barny, Alexander, Elixer, Zappa, Capone, Lear, Partner, Alceste, Ohio, Rockefeller, Johnny, Edward, and Gustav)[58]. To test this, we aligned the resistance gene enrichment sequencing (RenSeq) reads generated by Kale et al. (2022) from these cultivars to the GSTR 428 genome and confirmed the presence of all three *Lr28* genes in these lines based on gene-specific polymorphisms (Fig. 4c and Supplementary Fig. 19). Attraktion and the cultivar Robigus share the alien introgression on chromosome 4A by descent[58], prompting us to examine whether Robigus also carries the *Lr28* locus. Alignment of Robigus sequencing reads[60] to the GSTR 428 genome revealed the presence of all three *Lr28* genes in this cultivar (Supplementary Fig. 20a), which was further confirmed by PCR (Supplementary Fig. 20b).

Sequence analysis revealed that Attraktion, Robigus, and GSTR 428 share the same translocation breakpoint (Supplementary Fig. 21a, b). To further investigate the origin of the alien segment in Attraktion, we performed an average nucleotide identity (ANI) analysis[61], which revealed ~99.97% nucleotide identity between Attraktion and GSTR 428 across the distal 4AL region carrying *Lr28*, and sharp divergence in non-carrier genomes, including *T. dicoccoides* (Fig. 4d). These results indicate that the alien segment in Attraktion is derived from *Ae. speltoides*, not from *T. dicoccoides*.

Although obvious inversions were detected between Attraktion and GSTR 428 within the introgressed region (Supplementary Fig. 22a), Hi-C interaction heatmaps suggested that these are most likely attributable to assembly artifacts in the Attraktion genome rather than to genuine structural rearrangements (Supplementary Fig. 22b).

Minimizing the *Lr28* alien segment through *ph1b*-mediated recombination

To minimize potential linkage drag, we used the CS*ph1b* mutant to promote homoeologous recombination and generate lines carrying minimal introgressions (Fig. 5a). From the GSTR 428 × CS*ph1b* population, we obtained a resistant recombinant, designated *Lr28*-L6 (recombinant L6; Fig. 2a), carrying a markedly shortened alien segment. PCR marker analysis placed its proximal translocation breakpoint between markers *pku697* (744.26 Mb) and *pku715* (745.15 Mb), delimiting the retained alien segment to 14.10-14.99 Mb (GSTR 428 coordinates; Fig. 5a, b). A second round of *ph1b*-mediated recombination in selfed progeny of *Lr28*-L6 yielded *Lr28*-L6-224, with the distal breakpoint delimited to between markers *pku715* (745.15 Mb) and *pku095* (745.48 Mb), further reducing the alien segment to <1.22 Mb (Fig. 5b).

This recombinant *Lr28*-L6-224 was crossed and backcrossed three times with the spring wheat cultivar Yangmai 21 (YM21), which is susceptible to multiple *Pt* isolates[21]. BC_3F_2 progeny were genotyped with marker *pku715* to distinguish plants homozygous for the truncated *Lr28* segment from those lacking the introgression. Upon inoculation with five *Pt* pathotypes, the *Lr28*-carrying plants exhibited strong resistance, whereas non-introgressed plants were fully susceptible (Fig. 5c). Field trials under natural infection at Weifang (36°26'04.0"N, 119°26'42.6"E), Shandong, China during the 2025-2026 season further demonstrated that the BC_3F_3 line carrying the truncated segment (<1.22 Mb) conferred robust resistance, whereas its non-introgressed sister line remained susceptible (Fig. 5d).

DISCUSSION

Wild relatives of wheat, particularly *Ae. speltoides*, represent an invaluable reservoir of genetic diversity and resistance genes[21,62]. The all-stage leaf rust resistance gene *Lr28*, derived from *Ae. speltoides*, confers effective resistance against *Pt* and holds significant

potential for improving leaf rust resistance in wheat, particularly in regions where *Lr28* remains effective[46-49]. Despite its importance, the cloning of resistance genes from wild wheat relatives has long been hampered by suppressed recombination in alien introgression segments, and consequently, *Lr28* remained uncloned until now. Compounding this difficulty, *Lr28* originated from chromosome segment 7S#2 translocated into 4AL[40], adding another layer of complexity to its cloning. To overcome these challenges, we introduced the *ph1b* mutant to induce homoeologous recombination and assembled a high-quality reference genome (contig N50 = 101.48 Mb) for the introgression line GSTR 428 (Fig. 1c). This assembly not only facilitated the cloning of *Lr28* but also holds promise for accelerating the cloning of other *Lr* genes, as many of them have been transferred into the Thatcher genetic background.

Recent advances in EMS-based mutagenesis and cloning technologies, such as MutRenSeq[63], MutChromSeq[64], MutRNASeq[65], STAM[66], and MutIsoSeq[11], have enabled the cloning of numerous resistance genes. In our study, however, we found that the *Lr28* locus consists of three tandem *CNL* genes, each individually sufficient for resistance (Figs. 3 and 4a). This genetic architecture rendered conventional EMS-based cloning strategies ineffective for isolating *Lr28*, because the probability of simultaneously disrupting all three *CNL* genes through independent EMS-induced point mutations is extremely low. Consistent with this, only two susceptible mutants were identified from the EMS screen (Fig. 2c), both carrying segmental deletions within the introgressed 7S segment rather than point mutations in any single *CNL* gene. These observations support the functional redundancy of the three *CNL* genes against the tested pathotypes and explain why only segmental deletions could produce susceptibility.

The prevailing model of plant immunity describes singleton NLR proteins that recognize pathogen effectors and trigger immune responses[67]. However, accumulating evidence indicates that certain NLRs operate as sensor-helper pairs. In wheat, several sensor-helper pairs have recently been characterized, such as *TdNLR1*/*TdNLR2*, *CNL*/*NL*, *TdCNL1*/*TdCNL5*, $Yr6^{RL}$/$Yr6^{CNL1}$, and *RXL*/*Pm5e*[26-30]. Complementary NLR

pairs in the *Pm68* locus coordinately govern powdery mildew resistance[31-33]. Additionally, tandem kinase-NLR modules (e.g., *Sr62*^{TK}/*Sr62*^{NLR} and *WTK3*/*WTN1*) function as sensor-executor units[68,69]. Here, we report that the *Lr28* locus contains three tandem *CNL* genes—a genomic arrangement not previously documented in wheat. NBS-LRR gene clusters are known to evolve rapidly through ectopic recombination, resulting in frequent gene duplication and deletion events[70]. The high sequence similarity and tandem arrangement of *CNL1-CNL3* suggest that they arose through a recent duplication event, with limited time for functional divergence. The three-gene configuration may broaden the resistance spectrum, provide a genetic buffer against the loss any single gene, and serve as a reservoir for future neofunctionalization. Our findings thus add to the growing body of evidence highlighting the diverse and complex architectures of NLR-mediated resistance in plants.

The LRR domain is a major determinant of recognition specificity in plant NLR proteins and is subject to diversifying selection, which drives high levels of sequence polymorphism[71]. Lr28$^{CNL1/CNL2}$ and Lr28^{CNL3} share 99.03% identity, with 12 substitutions between them, 11 of which fall within the LRR domain (Fig. 2f), raising the possibility that the two proteins might recognize distinct effectors. However, when tested against seven Chinese *Pt* pathotypes, both genes displayed identical resistance profiles (Fig. 4a). Given the limited number of isolates examined, we cannot rule out the possibility that differences in specificity would emerge with a broader pathotype collection.

Our diagnostic marker screening revealed that *Lr28* is absent from most *T. turgidum* and *T. aestivum* genotypes examined (Supplementary Table 13) but is present in several European wheat cultivars (Fig. 4c). This distribution suggests that *Lr28* could benefit a wide range of commercial hexaploid and tetraploid wheat varieties, particularly in China, where leaf rust is a persistent threat and *Lr28* exhibits broadly effective resistance. The *Lr28*-carrying alien segment spans ~46.45 Mb in the GSTR 428 assembly. Such a large introgression may introduce linkage drag, potentially compromising agronomic performance. To enhance its breeding utility, we developed shortened recombinant lines (*Lr28*-L6-224, <1.22 Mb) via *ph1b*-mediated

homoeologous recombination (Fig. 5). Nevertheless, the presence of virulent isolates and the rapid evolution of pathogen populations pose challenges to the durability of *Lr28*-mediated resistance. Therefore, stacking *Lr28* with other resistance genes, such as *Lr34*[8], *Lr42*[20], *Lr47*[21], and *Lr67*[9], represents a more robust strategy for developing wheat cultivars with durable resistance. Collectively, the cloning of *Lr28*, the diagnostic marker, the shortened introgression lines, and the transfer of the resistance segment into the commercial cultivar YM21 represent an important step toward deploying *Lr28* in wheat breeding programs.

METHODS

Plant materials and genetic mapping

The introgression line GSTR 428 (Thatcher*6/*Ae. speltoides*), carrying the *Ae. speltoides* segment 7S#2, served as the source of the leaf rust resistance gene *Lr28*. A mapping population was generated by crossing GSTR 428 with the CS*ph1b* mutant, which promotes homoeologous recombination[72]. The *ph1b* deletion was confirmed using PCR markers *Xwmc2049* and *Xwmc2111*[73]. For initial phenotypic assessment, 15 F_1 and 122 F_2 plants from the GSTR 428 × CS*ph1b* cross were evaluated for resistance to *Pt* pathotype PHQS. For high-resolution genetic mapping, we selected 1,529 F_3 plants homozygous for the *ph1b* mutation and segregating for the *Lr28*-carrying alien segment. Plants with informative recombination events, along with their progeny, were subsequently inoculated with *Pt* pathotype PHQS. To validate the diagnostic marker for marker-assisted selection, we screened a diverse panel comprising 151 *T. aestivum*, 87 *T. turgidum*, and 94 *Ae. speltoides* accessions (Supplementary Table 13).

Leaf rust assays and pathogen growth assessment

Seedling rust response assays were performed at the Peking University Institute of Advanced Agricultural Sciences (Weifang, China) using ten *Pt* pathotypes: THDB, HCJR, PHQS, PHRT, PHTT, FHJR, PCJT, FHJL, THJT, and THTT (Supplementary Table 1). Fresh urediniospores of *Pt* were mixed with talcum powder (1:30) and inoculated onto seedlings at the three-leaf stage using a settling tower. Following inoculation, seedlings were kept in a dew chamber at 22 °C with 100% humidity for 24

h, and then moved to a growth chamber under a 16 h light/8 h dark photoperiod at 22 ± 2 °C. Disease reactions were evaluated ~12 dpi using a 0-4 scale[21], with scores of 0-2 classified as resistant and 3-4 as susceptible. For pathogen growth quantification, leaf segments from PHQS-inoculated GSTR 428 and Thatcher plants were harvested at 2, 4, 6, and 8 dpi, cleared in 10% KOH solution at 37 °C for 12 h, stained with WGA-FITC (Cat. No. L4895-10mg, Sigma-Aldrich, USA), and examined under a Zeiss Discovery V20 fluorescence dissecting microscope (Zeiss, Jena, Germany). Sporulation areas were quantified using ASSESS v.2 image analysis software[24]. Infection-focus areas were compared between GSTR 428 and Thatcher at each time point using two-tailed Student's *t*-tests, with $P < 0.05$ considered significant.

Cytological analysis

To characterize the alien chromatin, FISH and GISH were conducted at the Triticeae Research Institute, Sichuan Agricultural University. Chromosome preparations were obtained from root tip meristems using standard cytogenetic procedures. Oligonucleotide probes oligo-pSc119.2 and oligo-pTa535 were used for FISH to distinguish wheat and *Aegilops* chromosomes[21]. These probes were synthesized by TsingKe Biological Technology Co., Ltd. (Chengdu, Sichuan, China).

Genomic DNA sequencing and assembly

Fresh leaf tissue was collected from 10-day-old seedlings of GSTR 428, immediately flash-frozen in liquid nitrogen, and stored at -80 °C. Genomic DNA extraction, library construction, and sequencing were conducted by Berry Genomics Co., Ltd. (Beijing, China). Long-read sequencing was performed on the PacBio Revio platform to generate HiFi reads, and Hi-C libraries were constructed and sequenced on the MGI DNBSEQ-T7 platform. *De novo* assembly of HiFi reads was carried out using hifiasm v0.19.9 with "-l 0" parameters[74]. The resulting contigs were chromosome-anchored using Hi-C paired-end reads processed with 3D-DNA[75] and Juicer v1.6[76], followed by manual refinement in Juicebox v1.11 (https://github.com/aidenlab/Juicebox). Subsequently, gap filling was attempted with QuarTeT v1.2.1[77] with default settings. For assembly validation, raw HiFi reads were aligned to the final GSTR 428 genome using pbmm2 v1.10.0 (https://github.com/PacificBiosciences/pbmm2) with the "--preset HIFI"

parameter to evaluate mapping consistency.

Gene annotation

The GSTR 428 genome was annotated by integrating PacBio Iso-Seq, RNA-seq, and homology-based predictions. RNA was extracted from leaves, stems, spikes, and roots at the seedling and adult-plant stages (Supplementary Table 2). Library construction and sequencing were performed by Berry Genomics Co., Ltd. (Beijing, China). High-confidence gene models from the CS-IAAS reference genome[50] were transferred to the GSTR 428 assembly using Liftoff v1.6.3[78]. For evidence-based annotation, RNA-seq reads were trimmed and quality-filtered with fastp v0.23.2[79], aligned to the genome with HISAT2 v2.2.1[80], and assembled into transcripts with StringTie v2.2.1[81]. In parallel, Iso-Seq reads were processed through the Iso-Seq3 pipeline, mapped to the GSTR 428 genome with pbmm2 (https://github.com/PacificBiosciences/pbmm2), and collapsed into unique isoforms using cDNA_Cupcake (https://github.com/Magdoll/cDNA_Cupcake). Transcript assemblies from both RNA-seq and Iso-Seq data were merged with StringTie v2.2.1[81], and coding sequences were predicted with TransDecoder (https://github.com/TransDecoder/TransDecoder). All annotation files were consolidated into a single GFF3 file using the AGAT toolkit (https://github.com/NBISweden/AGAT). Transcript isoforms were clustered at the gene level with CD-HIT v4.8.1[82]. To ensure annotation quality, only gene models meeting at least one of the following criteria were retained as high-confidence: (i) significant homology to the UniProtKB Poaceae reference proteome (BLASTP e-value $\leq 1e^{-5}$, amino acid identity $\geq 80\%$, and query coverage $\geq 50\%$), or (ii) clear supporting evidence from RNA-seq data.

Assessment of genome assembly

Genome completeness was evaluated by searching for conserved single-copy orthologs in the *Poales_odb10* database using BUSCO v5.8.0[83]. Assembly quality was quantified using the LTR Assembly Index. Intact LTR retrotransposons were identified by LTR_FINDER_parallel v1.2[84] and LTR_retriever[85]. Per-base consensus quality values were estimated using Merqury v1.3[86].

Annotation of transposable elements

To annotate repetitive sequences, we first established a comprehensive transposable element library by combining de novo predictions generated with RepeatModeler2 v2.0.3[87] and curated reference sequences from the ClariTeRep database. This custom library was then used to identify and annotate transposable elements genome-wide with RepeatMasker v4.1.5[88].

Comparative genomic analysis

Pairwise whole-genome alignments of GSTR 428 against CS-IAAS and Attraktion were generated using MUMmer4[89]. The alignments were filtered with delta-filter to retain collinear blocks with ≥ 95% identity and a minimum length of 2 kb. Alignment coordinates were extracted using show-coords. Structural variants were identified using SyRI[90] and visualized with Plotsr v1.1.0[91].

Synteny analysis of chromosomes 4A, 5A, and 7B

To investigate structural variation and translocations involving chromosomes 4A, 5A, and 7B, we compared whole-genome protein sequences of *T. monococcum* (PI 306540), *T. aestivum* (CS-IAAS and GSTR 428), and *Ae. speltoides* (TS01 and Y2032). The longest transcript per gene was used for an all-vs-all BLASTP search (E-value ≤ $1e^{-5}$). The resulting candidate orthologous gene pairs were used as anchors to identify syntenic blocks using JCVI[92].

Coverage depth and polymorphism analysis

Whole-genome resequencing of Thatcher was performed by Berry Genomics Co., Ltd. (Beijing, China). Raw reads were trimmed with fastp v0.23.2[79] and aligned to the GSTR 428 genome with BWA-MEM v0.7.17[93]. Duplicates were marked with GATK v4.2.2.0[94] MarkDuplicates. Depth and coverage were calculated using SAMtools v1.19[95] and visualized in R. Variants were called with FreeBayes v1.3.6 (https://github.com/freebayes/freebayes) and filtered using BCFtools v1.14 (https://github.com/samtools/bcftools) to retain those with QUAL ≥ 30 and depth ≥ 5.

PCR marker development and screening

Genome-specific primers were designed using Primer3 (https://primer3.org/) to amplify gene regions encompassing putative specific SNPs. PCR reactions (20 μL) were performed on a Veriti 96-well thermal cycler (Applied Biosystems, CA, USA),

and amplicons were confirmed by Sanger sequencing. Restriction enzyme digestion was performed according to the manufacturer's protocol (New England Biolabs), and digested products were resolved on 1.5% agarose gels and visualized under UV light.

Microsynteny analysis

To investigate structural variation within the *Lr28* candidate interval, we performed microsynteny analysis across three *Ae. speltoides* accessions (AEG-9674-1, Y2032, and TS01)[52-54], GSTR 428, and CS-IAAS using JCVI[92]. Orthologs were identified by BLASTP (E-value ≤ $1e^{-5}$, C-score ≥ 0.99), and syntenic blocks were delineated with MCScanX (https://github.com/wyp1125/MCScanX).

EMS mutagenesis and mutant screening

Approximately 5,000 seeds of GSTR 428 were treated with 0.6% EMS (Sigma-Aldrich, M0880). Surviving plants were grown in a greenhouse, and 886 independent M_2 families were harvested. For each family, ~20 seedlings were inoculated with *Pt* pathotype PHQS. Susceptible M_2 plants were selfed, and their M_3 progeny were re-tested to confirm susceptibility. Genotyping with *Lr28*-linked genome-specific PCR markers (Supplementary Table 5) was performed to rule out seed contamination.

Differential expression analysis

Seedlings of GSTR 428 and Thatcher at the three-leaf stage were inoculated with *Pt* pathotype PHQS. Leaf samples were collected at 72 hpi, and immediately frozen in liquid nitrogen. Total RNA was extracted using the Spectrum Plant Total RNA Kit (Sigma-Aldrich, MA, USA). RNA-seq libraries were constructed by Berry Genomics Co., Ltd. (Beijing, China). Raw reads were trimmed with fastp v0.23.2[79], and transcript abundances were quantified via pseudo-alignment against the GSTR 428 reference transcriptome using kallisto v0.46.1[96]. Gene-level counts were obtained using the tximport package in R. Differential expression analysis was performed using DESeq2[97], and genes with FDR < 0.05, *p*-value < 0.05, and $|\log_2 \text{foldchange}| > 1$ were considered differentially expressed. Results were visualized using the pheatmap package in R.

CRISPR/Cas9-based gene editing

To validate the candidate genes *CNL1-CNL3* (*GSTR428.4A01G00526700*, *GSTR428.4A01G00526800*, and *GSTR428.4A01G00526900*), we used a

CRISPR/Cas9-based gene editing system. The fusion proteins Cas9-Trex2 and GRF4-GIF1 were used to enhance editing and regeneration efficiency. gRNAs were designed using the CRISPR-Cereal website (http://crispr.hzau.edu.cn/CRISPR-Cereal/index.php), and their specificity was verified by MUSCLE alignment and BLASTN searches against the GSTR 428 genome using the gRNA and PAM sequences as queries. The selected gRNA (5′-TTATGTGTGTGACTCTCGAA-3′) was synthesized, and the TaU3p-gRNA scaffold was generated through two rounds of PCR using pOPGR-TS1 as template[98] with primer pairs *Cas111-F1R1* and *Cas111-F2R2* (Supplementary Table 5). The resulting fragment was cloned into the modified pCas9T vector at the *Stu*I site using the In-Fusion® HD Cloning Kit (Clontech, CA, USA). The final construct was introduced into GSTR 428 via *Agrobacterium*-mediated transformation. Mutations in transgenic plants were identified using the gene-specific primer pairs *C720-CNL1-F1R1*, *C720-CNL2-F1R1*, and *C720-CNL3-F1R1* (Supplementary Table 5) and confirmed by Sanger sequencing.

Wheat genetic transformation

The full-length coding sequences of $Lr28^{CNL1}$ (identical to $Lr28^{CNL2}$) and $Lr28^{CNL3}$ were amplified from GSTR 428 cDNA using primer pairs *p1300-C721-F1R1* and *p1300-C722-F1R1* (Supplementary Table 5), and cloned into the GRF4-GIF1-containing pCAMBIA1300-OE vector driven by the maize UBI promoter. The resulting constructs were introduced into the spring wheat cultivar Fielder via *Agrobacterium*-mediated transformation. For complementation, genomic fragments of $Lr28^{CNL1}$ (8,056 bp) and $Lr28^{CNL3}$ (8,233 bp) were amplified from GSTR 428 genomic DNA using PrimeStar Max DNA Polymerase (TaKaRa, Kyoto, Japan) with primer pairs *p1300-C744-F1R1* and *p1300-C749-F1R1* (Supplementary Table 9). The 8,056-bp fragment comprised the full $Lr28^{CNL1}$ coding region (3,720 bp), along with 2,648 bp upstream of the start codon and 1,688 bp downstream of the stop codon. The 8,233-bp fragment contained the full $Lr28^{CNL3}$ coding region (3,720 bp), with 2,265 bp upstream and 2,248 bp downstream sequences. These fragments were cloned into the *Hind*III-HF/*Sac*I-HF linearized binary vector pCAMBIA1300, which carries the bialaphos resistance (*BAR*) selectable marker gene, using the In-Fusion® HD Cloning Kit

(Clontech, CA, USA). The resulting constructs were transformed into wheat cultivar Fielder. Transgene presence and expression were verified using primer pairs *Lr28F2R2* and *CNL-qPCR-F4R4* (Supplementary Table 5).

qRT-PCR analysis

Total RNA was extracted from leaves of transgenic T_0 plants at the three-leaf stage using the Spectrum Plant Total RNA Kit (Sigma-Aldrich, MA, USA), followed by purification with the Direct-zol RNA MiniPrepPlus Kit (ZymoResearch, CA, USA). qRT-PCR was carried out on an ABI QuantStudio 5 Real-Time PCR System (Applied Biosystems, CA, USA) using the primer pair *CNL-qPCR-F4R4* (Supplementary Table 5), with *TaActin* as the endogenous control[24]. Amplification products were separated on 1.5% agarose gels and imaged under UV light.

Haplotype and phylogenetic analysis

Homologs of $Lr28^{CNL1/CNL2}$ and $Lr28^{CNL3}$ were obtained from publicly available Triticeae genomes (http://plants.ensembl.org/ and https://wheatomics.sdau.edu.cn/) and the NCBI non-redundant database (http://www.ncbi.nlm.nih.gov/). Moreover, 94 *Ae. speltoides* accessions were inoculated with *Pt* pathotype PHQS, and the coding and 3′ UTR regions of $Lr28^{CNL1}$-$Lr28^{CNL3}$ were amplified using gene-specific primer pairs *Lr28-SHF-F1R1*, *Lr28-CNL1/2-SHF-F1R1*, *Lr28-CNL3-SHF-F1R1*, *Lr28-CNL1-SHF-F2R2*, *Lr28-CNL2-SHF-F2R2*, and *Lr28-CNL3-SHF-F3R3* (Supplementary Table 5), followed by Sanger sequencing. Sequences of previously cloned R proteins from Poaceae were downloaded from the NCBI database. Multiple alignments were generated with MUSCLE in MEGA7, and the phylogenetic tree was constructed using the neighbor-joining method with 1,000 bootstrap replicates. The resulting tree was visualized using iTOL v7 (https://itol.embl.de/).

Validation of the three *Lr28* genes in wheat cultivars by read alignment

Raw RenSeq data for 13 wheat cultivars (PRJEB48219) and whole-genome sequencing reads for cultivar Robigus (PRJEB35709) were downloaded from the European Nucleotide Archive (ENA). Reads were aligned to the GSTR 428 genome using BWA-MEM v0.7.17[93] with default parameters. Alignments were filtered using SAMtools v1.19[95] to retain reads with Number of Mismatches (NM) ≤ 3 (-e '[NM] <= 3'). The

644 filtered alignments were visualized in Integrative Genomics Viewer (https://igv.org/).

645 **Average nucleotide identity (ANI) analysis**

646 To evaluate the sequence similarity of the *Lr28*-carrying alien segments between
647 GSTR 428 and Attraktion[58], we performed an ANI analysis. Pairwise ANI values were
648 calculated using FastANI v1.34 (https://github.com/ParBLiSS/FastANI/releases), and
649 the resulting similarity matrix was visualized as a heatmap using the pheatmap package
650 in R.

651 **Hi-C-based validation of structural variants**

652 Raw Hi-C sequencing reads of Attraktion (PRJEB48529) were downloaded from the
653 ENA and aligned to the GSTR 428 genome using Juicer v1.6[76] with default parameters.
654 Hi-C contact maps were generated using 3D-DNA[75] and visualized in Juicebox v1.11
655 (https://github.com/aidenlab/Juicebox).

656 **Protein domain and structure prediction**

657 Domains of Lr28 proteins were predicted using the Conserved Domain Database at
658 NCBI (https://www.ncbi.nlm.nih.gov/cdd/). Their structures were predicted using
659 AlphaFold3 (https://alphafoldserver.com/) and visualized with PyMOL v3.1.5.1
660 (https://pymol.org/).

661 **Reduction of the *Ae. speltoides* alien segment**

662 GSTR 428 was crossed with CS*ph1b* to induce homoeologous recombination. A
663 recombinant line, *Lr28*-L6, carrying a truncated alien segment, was initially identified
664 during genetic mapping. This plant, which was heterozygous for *Lr28* and homozygous
665 for *ph1b*, was selfed to generate 432 F_4 progeny for a second round of recombination
666 screening. Using PCR markers *pku715* and *pku863*, we identified 16 new recombinant
667 individuals. Among these, plant No. 224 (designated *Lr28*-L6-224) carried a critical
668 recombination event between markers *pku715* (745.15 Mb) and *pku095* (745.48 Mb).
669 *Lr28*-L6-224 was crossed and backcrossed to the Chinese hexaploid wheat cultivar
670 YM21, which is susceptible to multiple *Pt* pathotypes[21]. Plants homozygous for the
671 shortened alien segment were subsequently selected using molecular markers and
672 evaluated for resistance to five *Pt* pathotypes. For field evaluation, BC_3F_3 sister lines
673 with or without the small introgressed segment (<1.22 Mb) were planted in 10 rows,

each 1.5 m in length.

Data availability

Data supporting the findings of this work are available within the paper and its supplementary information files. All raw sequencing data, genome assembly, and gene annotation generated in this project have been deposited at the National Genomics Data Center, Beijing Institute of Genomics, Chinese Academy of Sciences, under BioProject accession number PRJCA069012 (https://ngdc.cncb.ac.cn/gwh/Assembly/reviewer/OiWBKdtkdDKMubLTTyvknHLOrbfiuBFRERQSnMSMUKrmslLuzqZOaTseymMCyXhm). The GSTR 428 genome assembly and annotation are also available on Figshare (https://figshare.com/s/dca741f8341e2d7f5713). The sequences of *Lr28*^{CNL1}, *Lr28*^{CNL2}, and *Lr28*^{CNL3} have been deposited in NCBI GenBank under accession numbers PZ791522, PZ791523, and PZ791524. RenSeq raw data are available from the European Nucleotide Archive (ENA) under accession PRJEB48219. PacBio and Hi-C reads of Attraktion are available from the ENA under accession PRJEB48529. Whole-genome sequencing data of Robigus are available from the ENA under accession PRJEB35709. Source data are provided with this paper.

Code availability

All software packages used in the study are publicly available and as described in Methods and Reporting Summary.

Acknowledgements

We thank Dr. Yinghui Li (Sichuan Agricultural University) for providing seeds of the wheat cultivar Robigus. This research was supported by the National Natural Science Foundation of China (32472159), the Key R&D Program of Shandong Province (2024LZGC034 and 2024CXPT072), the State Key Laboratory of Crop Gene Exploration and Utilization in Southwest China (SKL-KF202409), the National Key Research and Development Program of China (2022YFD1201300), and the Taishan Scholars Program.

Author contributions

S.C. designed and supervised the project; L.Q., H.L., R.S., and Q.W. performed the experiments; S.u.R. contributed to genetic mapping; M.H. conducted cytogenetic assays; X.W. assisted with phenotyping; H.Y. assisted with the crossing and backcrossing experiments; Y.D. and P.Z. provided scientific support; S.C., H.L., and L.Q. analyzed the data. S.C., L.Q., H.L., and R.S. drafted the initial manuscript; S.C. generated the final manuscript. All authors reviewed and approved the manuscript.

Competing interests

S.C., H.L., L.Q., R.S., and S.u.R. are inventors on a Chinese provisional patent application (China patent filing No. 202611271684.8) relating to the use of the *Lr28* gene in wheat breeding programs. The remaining authors declare no competing interests.

References

1. Ray, D.K., Mueller, N.D., West, P.C. & Foley, J.A. Yield trends are insufficient to double global crop production by 2050. *PloS One* **8**, e66428 (2013).
2. Huerta-Espino, J. *et al.* Global status of wheat leaf rust caused by *Puccinia triticina*. *Euphytica* **179**, 143-160 (2011).
3. Singh, R.P. *et al.* Emergence and spread of new races of wheat stem rust fungus: continued threat to food security and prospects of genetic control. *Phytopathology* **105**, 872-884 (2015).
4. McIntosh, R.A., Wellings, C.R. & Park, R.F. *Wheat Rusts: an atlas of resistance genes* (CSIRO, 1995).
5. Ren, X. *et al.* Genetics of resistance to leaf rust in wheat: an overview in a genome-wide level. *Sustainability* **15**, 3247 (2023).
6. Sharma, D. *et al.* A single NLR gene confers resistance to leaf and stripe rust in wheat. *Nat Commun* **15**, 9925 (2024).
7. Yang, J. *et al.* Genome-assisted identification of wheat leaf rust resistance gene *Lr. ace-4A*/*Lr30*. *Nat Commun* **16**, 9339 (2025).
8. Krattinger, S.G. *et al.* A putative ABC transporter confers durable resistance to multiple fungal pathogens in wheat. *Science* **323**, 1360-1363 (2009).
9. Moore, J.W. *et al.* A recently evolved hexose transporter variant confers resistance to multiple pathogens in wheat. *Nat Genet* **47**, 1494-1498 (2015).
10. Cloutier, S. *et al.* Leaf rust resistance gene *Lr1*, isolated from bread wheat (*Triticum aestivum* L.) is a member of the large psr567 gene family. *Plant Mol*

Biol **65**, 93-106 (2007).
11. Wang, Y. *et al.* An unusual tandem kinase fusion protein confers leaf rust resistance in wheat. *Nat Genet* **55**, 914-920 (2023).
12. Feuillet, C. *et al.* Map-based isolation of the leaf rust disease resistance gene *Lr10* from the hexaploid wheat (*Triticum aestivum* L.) genome. *Proc Natl Acad Sci USA* **100**, 15253-8 (2003).
13. Hewitt, T. *et al.* Wheat leaf rust resistance gene *Lr13* is a specific *Ne2* allele for hybrid necrosis. *Mol Plant* **14**, 1025-1028 (2021).
14. Yan, X. *et al.* High-temperature wheat leaf rust resistance gene *Lr13* exhibits pleiotropic effects on hybrid necrosis. *Mol Plant* **14**, 1029-1032 (2021).
15. Kolodziej, M.C. *et al.* A membrane-bound ankyrin repeat protein confers race-specific leaf rust disease resistance in wheat. *Nat Commun* **12**, 956 (2021).
16. Huang, L. *et al.* Map-based cloning of leaf rust resistance gene *Lr21* from the large and polyploid genome of bread wheat. *Genetics* **164**, 655-664 (2003).
17. Thind, A.K. *et al.* Rapid cloning of genes in hexaploid wheat using cultivar-specific long-range chromosome assembly. *Nat Biotechnol* **35**, 793-796 (2017).
18. Lemmer, C. *et al.* Direct effector recognition by a tandem kinase triggers non-canonical immunity in wheat. *bioRxiv*, https://doi.org/10.64898/2026.02.17.706082 (2026).
19. Cavalet-Giorsa, E. *et al.* Origin and evolution of the bread wheat D genome. *Nature* **633**, 848-855 (2024).
20. Lin, G. *et al.* Cloning of the broadly effective wheat leaf rust resistance gene *Lr42* transferred from *Aegilops tauschii*. *Nat Commun* **13**, 3044 (2022).
21. Li, H. *et al.* Cloning of the wheat leaf rust resistance gene *Lr47* introgressed from *Aegilops speltoides*. *Nat Commun* **14**, 6072 (2023).
22. Li, Y., Govta, L., Sung, Y.-C., Coaker, G. & Fahima, T. The spectrum of diverse disease-resistance genes cloned and characterized in the Triticeae tribe. *Annu Rev Phytopathol* **63**, 175-200 (2025).
23. Chen, S., Zhang, W., Bolus, S., Rouse, M.N. & Dubcovsky, J. Identification and characterization of wheat stem rust resistance gene *Sr21* effective against the Ug99 race group at high temperature. *PLoS Genet* **14**, e1007287 (2018).
24. Zhang, W. *et al.* Identification and characterization of *Sr13*, a tetraploid wheat gene that confers resistance to the Ug99 stem rust race group. *Proc Natl Acad Sci USA* **114**, E9483-E9492 (2017).
25. Shen, T. *et al.* The wheat *Sr8155B1* gene encodes a typical NLR protein that confers resistance to the Ug99 stem rust race group. *Plant Commun* **6**, 101296 (2025).
26. Zhu, K. *et al.* An atypical NLR pair *TdCNL1*/*TdCNL5* from wild emmer confers powdery mildew resistance in wheat. *Nat Genet* **57**, 1553-1562 (2025).
27. Hu, Y. *et al.* A head-to-head NLR gene pair from wild emmer confers stripe rust resistance in wheat. *Nat Genet* **57**, 1543-1552 (2025).
28. Klymiuk, V. *et al.* Coordinated function of paired NLRs confers *Yr84*-mediated stripe rust resistance in wheat. *Nat Genet* **57**, 1535-1542 (2025).
29. Sun, W. *et al.* The wheat *Yr6* locus, allelic to *Pm5*, harbors an NLR gene pair

conferring stripe rust resistance. *Plant Commun* **7**, 101541 (2026).
30. Guo, G. *et al.* The wheat NLR pair *RXL*/*Pm5e* confers resistance to powdery mildew. *Plant Biotechnol J* **23**, 1260-1276 (2025).
31. Zhang, H. *et al.* Paired NLRs originated from *Triticum dicoccoides* coordinately confer resistance to powdery mildew in wheat. *Nat Commun* **16**, 9040 (2025).
32. Yang, Z. *et al.* Two complementary NLRs from wild emmer wheat confer powdery mildew resistance. *Nat Commun* **16**, 9041 (2025).
33. He, H. *et al.* An NLR pair in the *Pm68* locus confers powdery mildew resistance in durum and common wheat. *Nat Commun* **16**, 9039 (2025).
34. Bolton, M.D., Kolmer, J.A. & Garvin, D.F. Wheat leaf rust caused by *Puccinia triticina*. *Mol Plant Pathol* **9**, 563-575 (2008).
35. McCallum, B.D. *et al.* A review of wheat leaf rust research and the development of resistant cultivars in Canada. *Can J Plant Pathol* **38**, 1-18 (2016).
36. Miki, Y. *et al.* Origin of wheat B-genome chromosomes inferred from RNA sequencing analysis of leaf transcripts from section *Sitopsis* species of *Aegilops*. *DNA Res* **26**, 171-182 (2019).
37. Dubcovsky, J., Lukaszewski, A., Echaide, M., Antonelli, E. & Porter, D. Molecular characterization of two *Triticum speltoides* interstitial translocations carrying leaf rust and greenbug resistance genes. *Crop Sci* **38**, 1655-1660 (1998).
38. Marais, G. *et al.* Attempts to remove gametocidal genes co-transferred to common wheat with rust resistance from *Aegilops speltoides*. *Euphytica* **171**, 71-85 (2010).
39. Riley, R., Chapman, V. & Johnson, R. The incorporation of alien disease resistance in wheat by genetic interference with the regulation of meiotic chromosome synapsis. *Genet Res* **12**, 199-219 (1968).
40. Friebe, B., Jiang, J., Raupp, W., McIntosh, R. & Gill, B. Characterization of wheat-alien translocations conferring resistance to diseases and pests: current status. *Euphytica* **91**, 59-87 (1996).
41. Tomar, S. & Menon, M. Introgression of alien genes for leaf rust (*Puccinia recondita*) resistance into bread wheat (*Triticum aestivum*) cultivars. *Indian J Agric Sci* **68**, 675–681 (1998).
42. Sohail, Y. *et al.* Identification of a co-dominant eSTS marker linked with leaf rust resistance gene *Lr28* in wheat (*Triticum aestivum* L.). *Aust J Crop Sci* **8**, 1210-1215 (2014).
43. Cherukuri, D.P. *et al.* Molecular mapping of *Aegilops speltoides* derived leaf rust resistance gene *Lr28* in wheat. *Euphytica* **143**, 19-26 (2005).
44. Bhardwaj, S. *et al.* Virulence of *Puccinia triticina* on *Lr28* in wheat and its evolutionary relation to prevalent pathotypes in India. *Cereal Res Commun* **38**, 83-89 (2010).
45. Lind, V. & Gultyaeva, E. Virulence frequencies of *Puccinia triticina* in Germany and the European regions of the Russian Federation. *J Phytopathol* **155**, 13-21 (2007).
46. Prasad, P. *et al.* Population differentiation of wheat leaf rust fungus *Puccinia triticina* in South Asia. *Curr Sci* **112**, 2073-2084 (2017).

47. Skolotneva, E. *et al.* Effectiveness of leaf rust resistance genes against *Puccinia triticina* populations in Western Siberia during 2008–2017. *J Plant Dis Prot* **125**, 549-555 (2018).
48. Gebrewahid, T.W., Yao, Z.-J., Yan, X.-C., Gao, P. & Li, Z.-F. Identification of leaf rust resistance genes in Chinese common wheat cultivars. *Plant Dis* **101**, 1729-1737 (2017).
49. Zhang, L. *et al.* Race and virulence analysis of *Puccinia triticina* in China in 2014 and 2015. *Plant Dis* **104**, 455-464 (2020).
50. Liu, S. *et al.* A telomere-to-telomere genome assembly coupled with multi-omic data provides insights into the evolution of hexaploid bread wheat. *Nat Genet* **57**, 1008-1020 (2025).
51. Dvorak, J. *et al.* Reassessment of the evolution of wheat chromosomes 4A, 5A, and 7B. *Theor Appl Genet* **131**, 2451-2462 (2018).
52. Li, L.-F. *et al.* Genome sequences of five Sitopsis species of *Aegilops* and the origin of polyploid wheat B subgenome. *Mol Plant* **15**, 488-503 (2022).
53. Avni, R. *et al.* Genome sequences of three *Aegilops* species of the section Sitopsis reveal phylogenetic relationships and provide resources for wheat improvement. *Plant J* **110**, 179-192 (2022).
54. Yang, Y. *et al.* Genome sequencing of Sitopsis species provides insights into their contribution to the B subgenome of bread wheat. *Plant Commun* **4**, 100567 (2023).
55. Pan, W. *et al.* Efficient gene disruption in polyploid genome by Cas9-Trex2 fusion protein. *J Integr Plant Biol* **67**, 7-10 (2025).
56. Debernardi, J.M. *et al.* A GRF–GIF chimeric protein improves the regeneration efficiency of transgenic plants. *Nat Biotechnol* **38**, 1274-1279 (2020).
57. Liu, F. *et al.* Exome association analysis sheds light onto leaf rust (*Puccinia triticina*) resistance genes currently used in wheat breeding (*Triticum aestivum* L.). *Plant Biotechnol J* **18**, 1396-1408 (2020).
58. Kale, S.M. *et al.* A catalogue of resistance gene homologs and a chromosome-scale reference sequence support resistance gene mapping in winter wheat. *Plant Biotechnol J* **20**, 1730-1742 (2022).
59. Przewieslik-Allen, A.M. *et al.* The role of gene flow and chromosomal instability in shaping the bread wheat genome. *Nat Plants* **7**, 172-183 (2021).
60. Walkowiak, S. *et al.* Multiple wheat genomes reveal global variation in modern breeding. *Nature* **588**, 277-283 (2020).
61. Wang, X. *et al.* A near-complete genome sequence of einkorn wheat provides insight into the evolution of wheat A subgenomes. *Plant Commun* **5**, 100768 (2024).
62. Mago, R. *et al.* Development of wheat–*Aegilops speltoides* recombinants and simple PCR-based markers for *Sr32* and a new stem rust resistance gene on the 2S#1 chromosome. *Theor Appl Genet* **126**, 2943-2955 (2013).
63. Steuernagel, B. *et al.* Rapid cloning of disease-resistance genes in plants using mutagenesis and sequence capture. *Nat Biotechnol* **34**, 652-655 (2016).
64. Sánchez-Martín, J. *et al.* Rapid gene isolation in barley and wheat by mutant

chromosome sequencing. *Genome Biol* **17**, 221 (2016).
65. Yu, G. *et al. Aegilops sharonensis* genome-assisted identification of stem rust resistance gene *Sr62*. *Nat Commun* **13**, 1607 (2022).
66. Ni, F. *et al.* Sequencing trait-associated mutations to clone wheat rust-resistance gene *YrNAM*. *Nat Commun* **14**, 4353 (2023).
67. Förderer, A. *et al.* A wheat resistosome defines common principles of immune receptor channels. *Nature* **610**, 532-539 (2022).
68. Lu, P. *et al.* A wheat tandem kinase and NLR pair confers resistance to multiple fungal pathogens. *Science* **387**, 1418-1424 (2025).
69. Chen, R. *et al.* A wheat tandem kinase activates an NLR to trigger immunity. *Science* **387**, 1402-1408 (2025).
70. Richter, T.E. & Ronald, P.C. The evolution of disease resistance genes. *Plant Mol Biol* **42**, 195-204 (2000).
71. Dodds, P.N. *et al.* Direct protein interaction underlies gene-for-gene specificity and coevolution of the flax resistance genes and flax rust avirulence genes. *Proc Natl Acad Sci USA* **103**, 8888-8893 (2006).
72. Xu, B. *et al.* Mapping and characterization of rust resistance genes *Lr53* and *Yr35* introgressed from *Aegilops* species. *Theor Appl Genet* **137**, 113 (2024).
73. Gyawali, Y., Zhang, W., Chao, S., Xu, S. & Cai, X. Delimitation of wheat *ph1b* deletion and development of *ph1b*-specific DNA markers. *Theor Appl Genet* **132**, 195-204 (2019).
74. Cheng, H., Concepcion, G.T., Feng, X., Zhang, H. & Li, H. Haplotype-resolved de novo assembly using phased assembly graphs with hifiasm. *Nat Methods* **18**, 170-175 (2021).
75. Dudchenko, O. *et al.* De novo assembly of the *Aedes aegypti* genome using Hi-C yields chromosome-length scaffolds. *Science* **356**, 92-95 (2017).
76. Durand, N.C. *et al.* Juicer provides a one-click system for analyzing loop-resolution Hi-C experiments. *Cell Syst* **3**, 95-98 (2016).
77. Lin, Y. *et al.* quarTeT: a telomere-to-telomere toolkit for gap-free genome assembly and centromeric repeat identification. *Hortic Res* **10**, uhad127 (2023).
78. Shumate, A., Salzberg, S.L. & Valencia, A. Liftoff: accurate mapping of gene annotations. *Bioinformatics* **37**, 1639-1643 (2021).
79. Chen, S., Zhou, Y., Chen, Y. & Gu, J. fastp: an ultra-fast all-in-one FASTQ preprocessor. *Bioinformatics* **34**, i884-i890 (2018).
80. Kim, D., Langmead, B. & Salzberg, S.L. HISAT: a fast spliced aligner with low memory requirements. *Nat Methods* **12**, 357-360 (2015).
81. Pertea, M., Kim, D., Pertea, G.M., Leek, J.T. & Salzberg, S.L. Transcript-level expression analysis of RNA-seq experiments with HISAT, StringTie and Ballgown. *Nat Protoc* **11**, 1650-1667 (2016).
82. Fu, L., Niu, B., Zhu, Z., Wu, S. & Li, W. CD-HIT: accelerated for clustering the next-generation sequencing data. *Bioinformatics* **28**, 3150-3152 (2012).
83. Simão, F.A., Waterhouse, R.M., Ioannidis, P., Kriventseva, E.V. & Zdobnov, E.M. BUSCO: assessing genome assembly and annotation completeness with single-copy orthologs. *Bioinformatics* **31**, 3210-3212 (2015).

84. Ou, S. & Jiang, N. LTR_FINDER_parallel: parallelization of LTR_FINDER enabling rapid identification of long terminal repeat retrotransposons. *Mobile DNA* **10**, 48 (2019).
85. Ou, S. & Jiang, N. LTR_retriever: a highly accurate and sensitive program for identification of long terminal repeat retrotransposons. *Plant Physiol* **176**, 1410-1422 (2018).
86. Rhie, A., Walenz, B.P., Koren, S. & Phillippy, A.M. Merqury: reference-free quality, completeness, and phasing assessment for genome assemblies. *Genome Biol* **21**, 245 (2020).
87. Flynn, J.M. *et al.* RepeatModeler2 for automated genomic discovery of transposable element families. *Proc Natl Acad Sci USA* **117**, 9451-9457 (2020).
88. Tarailo-Graovac, M. & Chen, N. Using RepeatMasker to identify repetitive elements in genomic sequences. *Curr Protoc Bioinformatics* **25**, 4.10.1-4.10.14 (2009).
89. Marçais, G. *et al.* MUMmer4: A fast and versatile genome alignment system. *PLoS Comput Biol* **14**, e1005944 (2018).
90. Goel, M., Sun, H., Jiao, W.-B. & Schneeberger, K. SyRI: finding genomic rearrangements and local sequence differences from whole-genome assemblies. *Genome Biol* **20**, 277 (2019).
91. Goel, M. & Schneeberger, K. Plotsr: visualizing structural similarities and rearrangements between multiple genomes. *Bioinformatics* **38**, 2922-2926 (2022).
92. Tang, H. *et al.* JCVI: A versatile toolkit for comparative genomics analysis. *iMeta* **3** (2024).
93. Li, H. & Durbin, R. Fast and accurate short read alignment with Burrows–Wheeler transform. *Bioinformatics* **25**, 1754-1760 (2009).
94. McKenna, A. *et al.* The Genome Analysis Toolkit: a MapReduce framework for analyzing next-generation DNA sequencing data. *Genome Res* **20**, 1297-303 (2010).
95. Li, H. *et al.* The Sequence Alignment/Map format and SAMtools. *Bioinformatics* **25**, 2078-2079 (2009).
96. Bray, N.L., Pimentel, H., Melsted, P. & Pachter, L. Near-optimal probabilistic RNA-seq quantification. *Nat Biotechnol* **34**, 525-527 (2016).
97. Anders, S. & Huber, W. Differential analysis of count data–the DESeq2 package. *Genome Biol* **15**, 550 (2014).
98. Li, J., Wang, Z., He, G., Ma, L. & Deng, X.W. CRISPR/Cas9-mediated disruption of *TaNP1* genes results in complete male sterility in bread wheat. *J Genet Genomics* **47**, 263-272 (2020).

Figure Legends

Fig. 1. Characterization of the introgressed alien segment and genome assembly of GSTR 428. a, Seedling responses of GSTR 428 and Thatcher after inoculation with ten Chinese *Pt* pathotypes (Supplementary Table 1). R, resistant; S, susceptible. **b**, Cytogenetic validation by GISH and FISH, confirming an alien translocation in GSTR 428. White arrows indicate the introgressed alien segment. **c**, Circos plot of the GSTR 428 genome assembly. Rings from outside to inside: (I) chromosomes, (II) GC content, (III) gene density, (IV) *Gypsy* density, (V) *Copia* density, (VI) syntenic links. **d**, Synteny analysis between GSTR 428 and the CS-IAAS reference genome. Inversions are highlighted in yellow, and translocations in blue. **e**, Syntenic blocks among *T. monococcum* (PI 306540), *Ae. speltoides* (TS01 and Y2032), and bread wheat (CS-IAAS and GSTR 428). Each line represents a syntenic block composed of ≥20 collinear gene pairs with ≥80% sequence similarity. Green lines highlight syntenic regions corresponding to the alien 7S#2 segment. **f**, Identification of the translocation breakpoint in GSTR 428. Coverage depth (top) and distribution of called variants (bottom) of Thatcher resequencing reads aligned to the GSTR 428 genome, calculated in 50-kb sliding windows. Black arrows indicate the translocation breakpoint.

Fig. 2. Genetic mapping and candidate gene identification for *Lr28*. a, Genetic mapping of *Lr28* based on the GSTR 428 genome. Blue bars denote *Ae. speltoides* segments; yellow arrows indicate NLR genes. **b**, Collinearity analysis of the *Lr28* candidate interval across GSTR 428, three *Ae. speltoides* accessions (AEG-9674-1, Y2032, and TS01), and CS-IAAS. **c**, Infection phenotypes of the susceptible EMS mutants. R, resistant; S, susceptible. **d**, Read-depth coverage plots for resequencing data of M56 and M473 aligned to the GSTR 428 reference genome, calculated in 50-kb sliding windows. **e**, Heatmap showing gene expression profiles within the *Lr28* candidate region, derived from RNA-seq data of GSTR 428 and Thatcher at 72 hpi with PHQS. **f**, Protein domain architectures and sequence polymorphisms of the three *Lr28* candidate genes. The coiled-coil (CC), nucleotide-

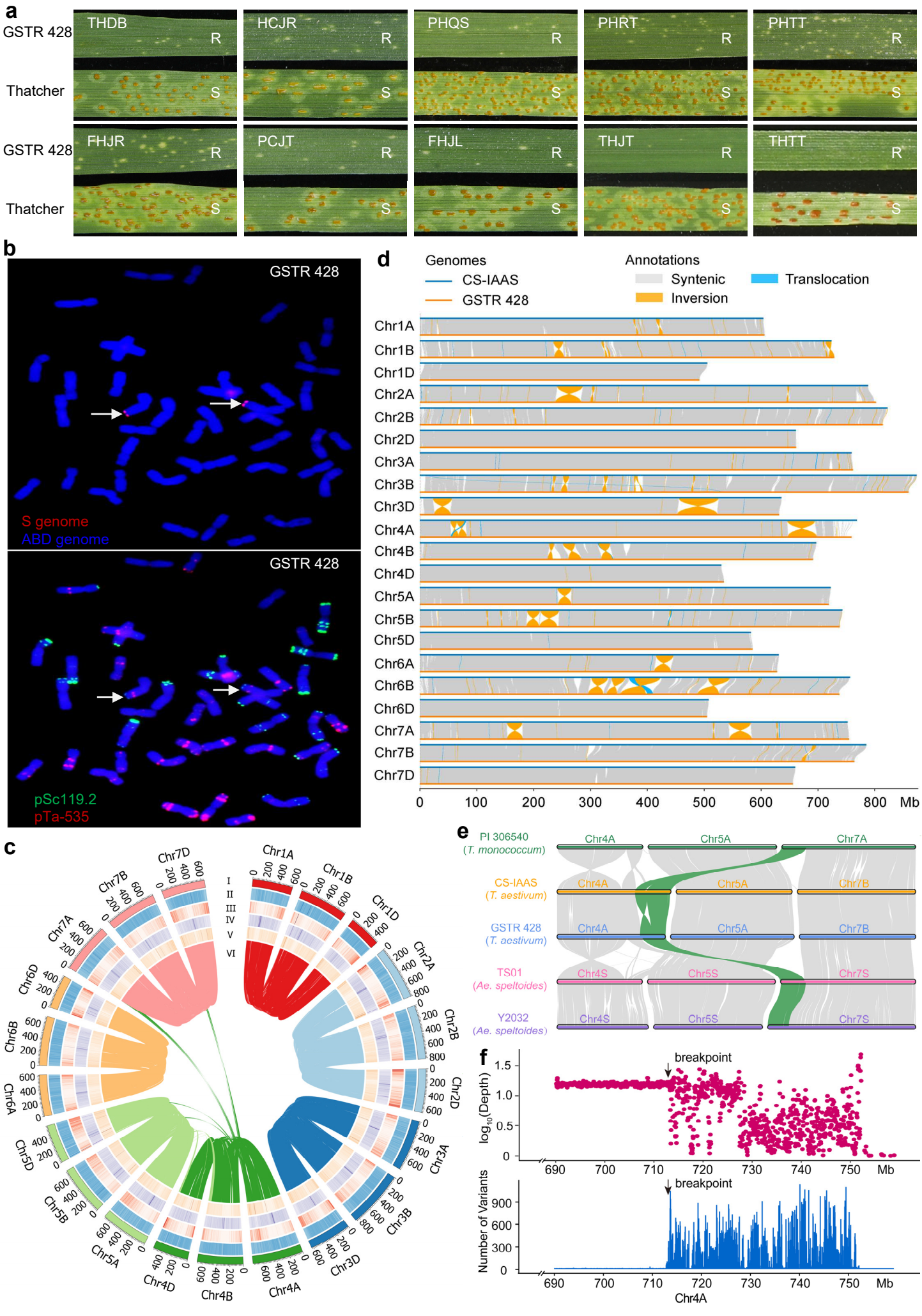
binding (NB-ARC), and leucine-rich repeat (LRR) domains are highlighted in yellow, green, and pink, respectively; blue denotes the remaining non-domain regions.

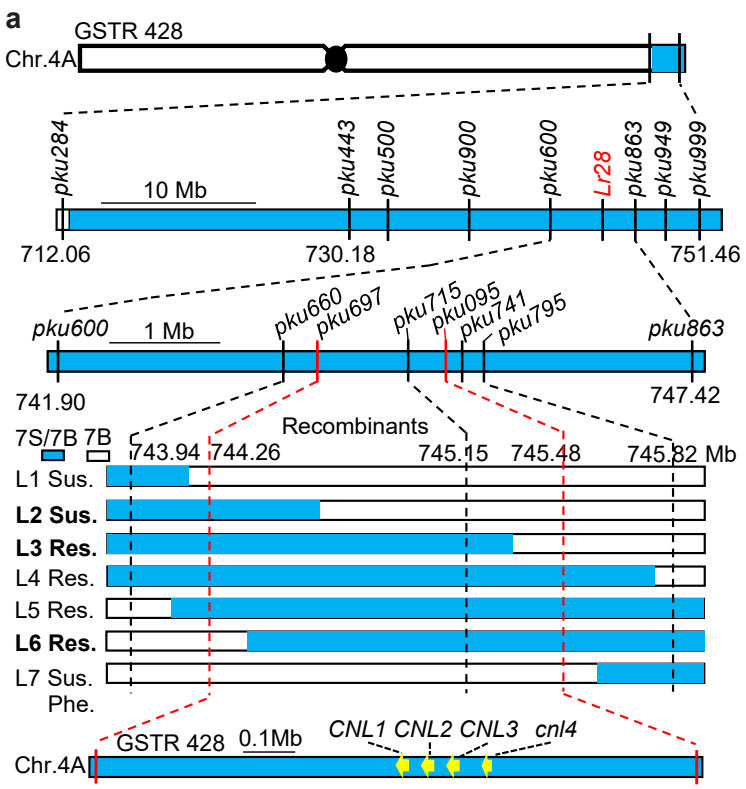
Fig. 3. Functional validation of candidate genes via CRISPR/Cas9 editing and transgenic experiments. a, Sequencing chromatograms of GSTR 428 and five CRISPR/Cas9-edited mutants (T_0KO-1, T_0KO-2, T_1KO-3, T_1KO-4, and T_1KO-5). The red box indicates the gRNA target site; the PAM sequence is highlighted in red; dashes denote deleted bases. **b**, Infection phenotypes of representative T_0 edited plants carrying loss-of-function mutations in all three *CNL* genes simultaneously. **c,** Infection phenotypes of T_1 progeny carrying loss-of-function mutations either in all three *CNL* genes or in only one of the three genes. **d**, **e**, Schematic diagrams of overexpression constructs for *CNL1*/*CNL2* (d) and *CNL3* (e). Black arrows indicate coding regions; LB and RB denote the left and right T-DNA borders, respectively. **f**, **g**, Infection phenotypes of T_1 plants overexpressing *CNL1*/*CNL2* (f) and *CNL3* (g) in the Fielder background. **h**, **i**, Schematic diagrams of genomic fragments carrying *CNL1* (h) and *CNL3* (i) used for transgenic complementation. Black arrows indicate coding regions, and their native regulatory sequences are indicated below each diagram. **j**, **k**, Infection phenotypes of T_1 plants expressing native *CNL1* (j) and *CNL3* (k) in the Fielder background. -, transgene absent; +, transgene present; R, resistant; S, susceptible.

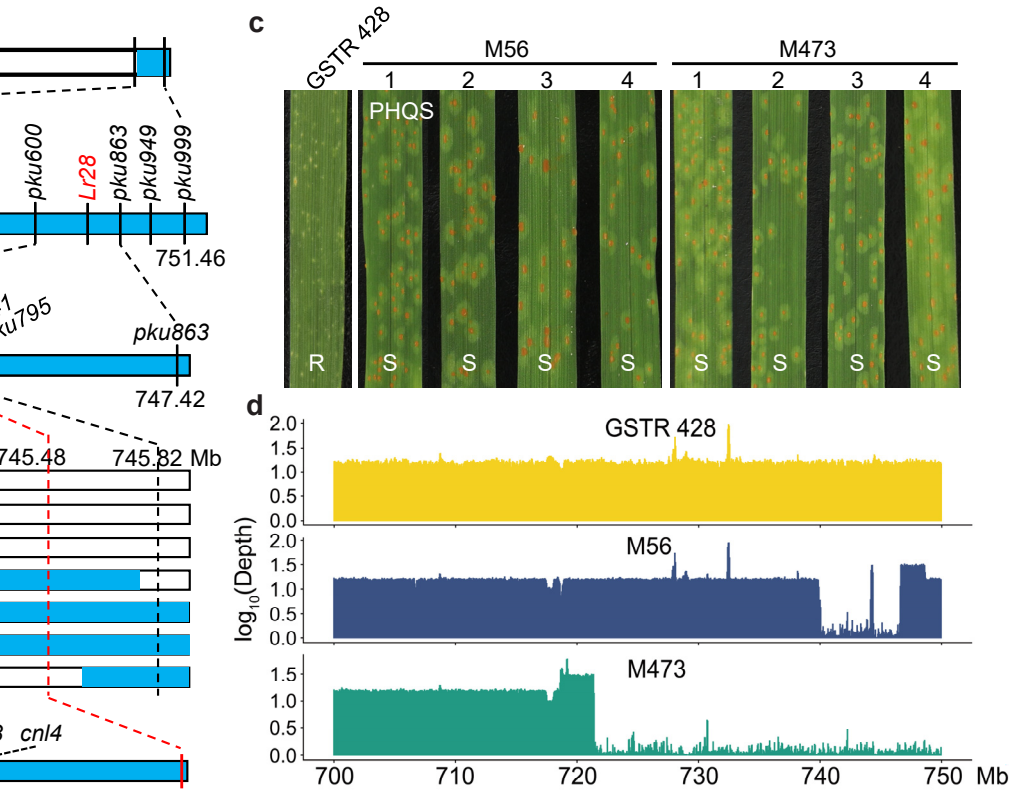
Fig. 4. Characterization and haplotyping of the *Lr28* genes and their relationship to the 4AL GWAS resistance locus. a, Infection phenotypes of independent T_1 overexpression lines for $Lr28^{CNL1/CNL2}$ (T_1C721-6 and T_1C721-8) and $Lr28^{CNL3}$ (T_1C722-1 and T_1C722-5) inoculated with seven *Pt* pathotypes. **b**, Protein polymorphisms among *Lr28* haplotypes. Light blue indicates polymorphisms shared with $Lr28^{CNL3}$; light orange indicates additional amino acid differences absent in both $Lr28^{CNL1/CNL2}$ and $Lr28^{CNL3}$. **c**, Integrative Genomics Viewer snapshots showing RenSeq reads from 13 wheat cultivars aligned to the three *Lr28* genes. Red lines indicate gene-specific polymorphisms. **d**, ANI analysis of the alien segment

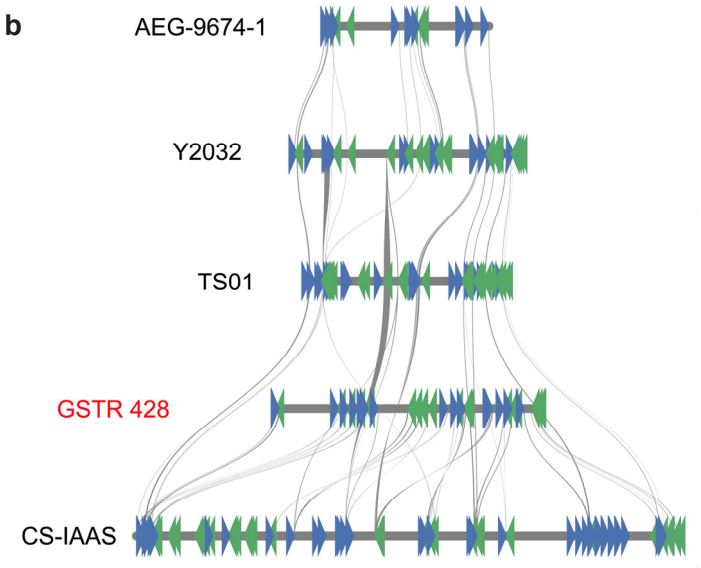
harboring *Lr28*. The distal region of chromosome arm 4AL (indicated by a black arrow) was compared between GSTR 428 and 11 additional wheat genomes. ANI values are represented by a color gradient from blue (<94%) through white to red (100%).

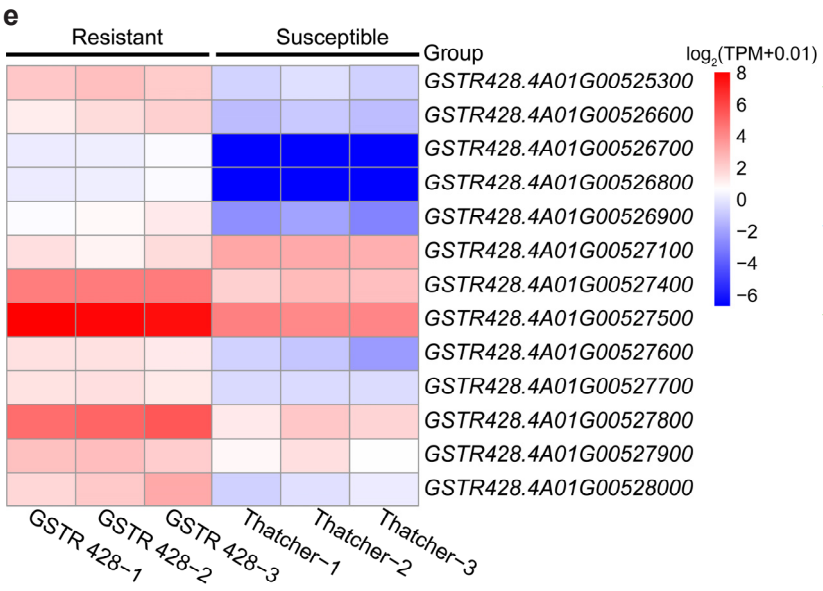
Fig. 5. Minimization of the *Lr28*-carrying introgression segment and its transfer into wheat cultivar YM21. a, Workflow for reducing the alien segment harboring *Lr28* and subsequently transferring the truncated fragment into the spring wheat cultivar YM21. Chromatin lengths are estimated based on the GSTR 428 genome assembly. **b**, Schematic representation of stepwise reduction of the introgressed *Ae. speltoides* segment carrying *Lr28*. Blue bars denote the introgressed alien chromatin; PCR markers are listed in Supplementary Table 5. **c**, Disease reactions of sister lines carrying (+) or lacking (-) the truncated *Lr28*-containing segment in response to five *Pt* pathotypes. R, resistant; S, susceptible. **d**, Field performance of the introgression line YM21+ *Lr28*-L6-224 (*Lr28*) and its non-introgressed sister line (*lr28*) under natural disease pressure.

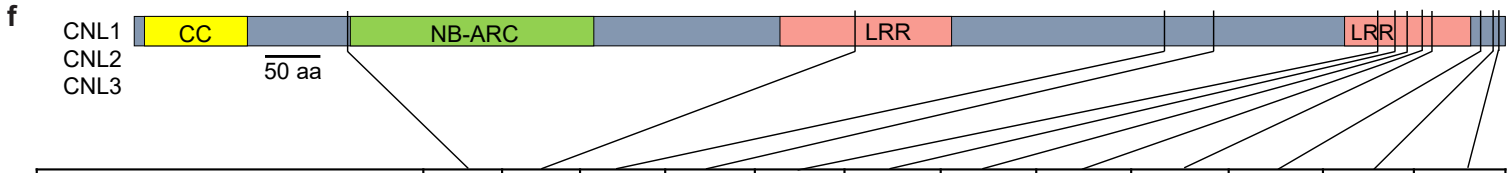

a
GSTR 428
Thatcher
GSTR 428
Thatcher
THDB
HCJR
PHQS
PHRT
PHTT
FHJR
PCJT
FHJL
THJT
THTT
R
S
b
GSTR 428
S genome
ABD genome
GSTR 428
pSc119.2
pTa-535
c
Chr1A
Chr1B
Chr1D
Chr2A
Chr2B
Chr2D
Chr3A
Chr3B
Chr3D
Chr4A
Chr4B
Chr4D
Chr5A
Chr5B
Chr5D
Chr6A
Chr6B
Chr6D
Chr7A
Chr7B
Chr7D
I
II
III
IV
V
VI
d
Genomes
CS-IAAS
GSTR 428
Annotations
Syntenic
Inversion
Translocation
Chr1A
Chr1B
Chr1D
Chr2A
Chr2B
Chr2D
Chr3A
Chr3B
Chr3D
Chr4A
Chr4B
Chr4D
Chr5A
Chr5B
Chr5D
Chr6A
Chr6B
Chr6D
Chr7A
Chr7B
Chr7D
0
100
200
300
400
500
600
700
800
Mb
e
PI 306540
(T. monococcum)
CS-IAAS
(T. aestivum)
GSTR 428
(T. aestivum)
TS01
(Ae. speltoides)
Y2032
(Ae. speltoides)
Chr4A
Chr5A
Chr7A
Chr4A
Chr5A
Chr7B
Chr4A
Chr5A
Chr7B
Chr4S
Chr5S
Chr7S
Chr4S
Chr5S
Chr7S
f
breakpoint
log10(Depth)
1.5
1.0
0.5
0
690
700
710
720
730
740
750
Mb
breakpoint
Number of Variants
900
600
300
0
690
700
710
720
730
740
750
Mb
Chr4A



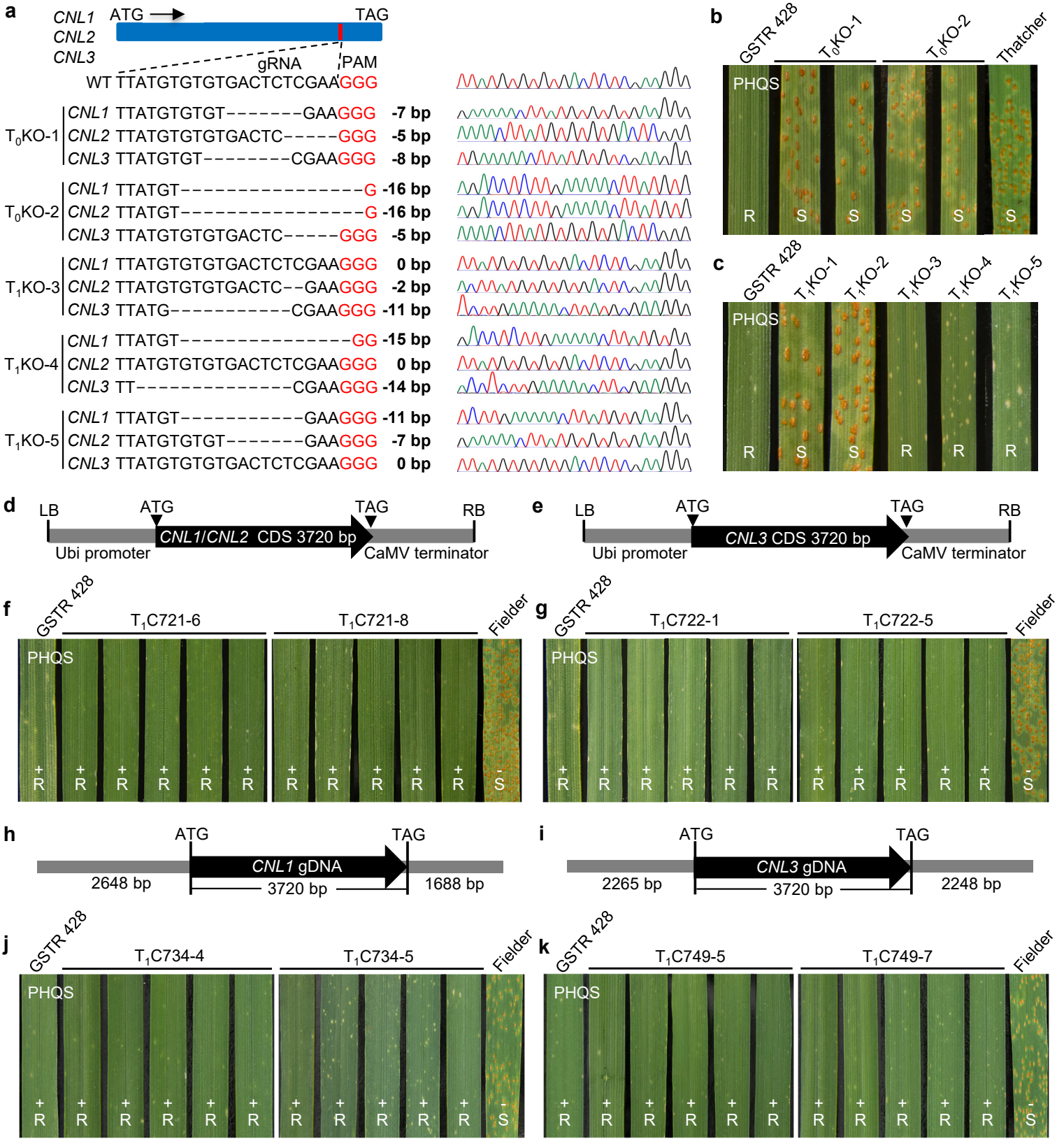




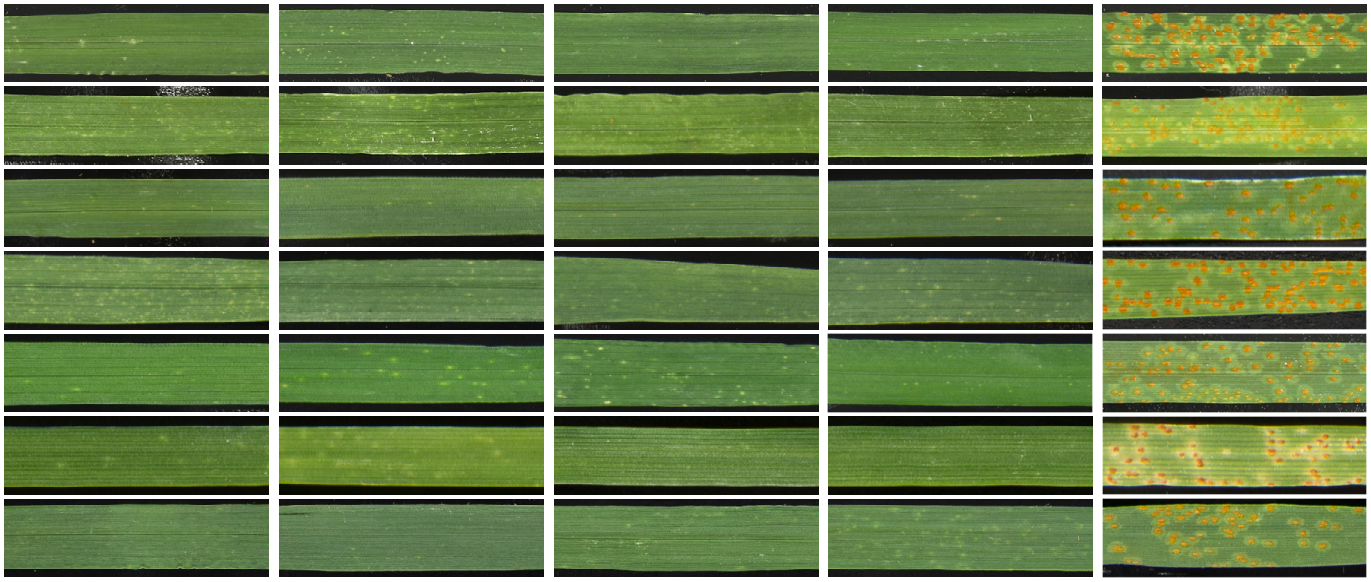




Position (aa)	193	652	932	976	1137	1153	1164	1178	1186	1217	1229	1233
CNL1: GSTR428.4A01G00526700	Leu	Thr	Phe	Trp	Arg	Thr	Arg	Ser	Ala	Arg	Ile	Thr
CNL2: GSTR428.4A01G00526800	Leu	Thr	Phe	Trp	Arg	Thr	Arg	Ser	Ala	Arg	Ile	Thr
CNL3: GSTR428.4A01G00526900	Phe	Ala	Leu	Arg	Gly	Ala	Lys	Glu	Gly	Ile	Val	Arg


a
CNL1
CNL2
CNL3
ATG
TAG
gRNA
PAM
WT TTATGTGTGTGACTCTCGAAGGG
T0KO-1
CNL1 TTATGTGTGT-------GAAGGG -7 bp
CNL2 TTATGTGTGTGACTC-----GGG -5 bp
CNL3 TTATGTGT--------CGAAGGG -8 bp
T0KO-2
CNL1 TTATGT----------------G -16 bp
CNL2 TTATGT----------------G -16 bp
CNL3 TTATGTGTGTGACTC-----GGG -5 bp
T1KO-3
CNL1 TTATGTGTGTGACTCTCGAAGGG 0 bp
CNL2 TTATGTGTGTGACTC--GAAGGG -2 bp
CNL3 TTATG----------CGAAGGG -11 bp
T1KO-4
CNL1 TTATGT--------------GG -15 bp
CNL2 TTATGTGTGTGACTCTCGAAGGG 0 bp
CNL3 TT--------------CGAAGGG -14 bp
T1KO-5
CNL1 TTATGT----------GAAGGG -11 bp
CNL2 TTATGTGTGT-------GAAGGG -7 bp
CNL3 TTATGTGTGTGACTCTCGAAGGG 0 bp
b
GSTR 428
T0KO-1
T0KO-2
Thatcher
PHQS
R S S S S S
c
GSTR 428
T1KO-1
T1KO-2
T1KO-3
T1KO-4
T1KO-5
PHQS
R S S R R R
d
LB
ATG
TAG
RB
CNL1/CNL2 CDS 3720 bp
Ubi promoter
CaMV terminator
e
LB
ATG
TAG
RB
CNL3 CDS 3720 bp
Ubi promoter
CaMV terminator
f
GSTR 428
T1C721-6
T1C721-8
Fielder
PHQS
+R +R +R +R +R +R +R +R +R +R +R -S
g
GSTR 428
T1C722-1
T1C722-5
Fielder
PHQS
+R +R +R +R +R +R +R +R +R +R +R -S
h
ATG
TAG
CNL1 gDNA
2648 bp
3720 bp
1688 bp
i
ATG
TAG
CNL3 gDNA
2265 bp
3720 bp
2248 bp
j
GSTR 428
T1C734-4
T1C734-5
Fielder
PHQS
+R +R +R +R +R +R +R +R +R +R +R -S
k
GSTR 428
T1C749-5
T1C749-7
Fielder
PHQS
+R +R +R +R +R +R +R +R +R +R +R -S

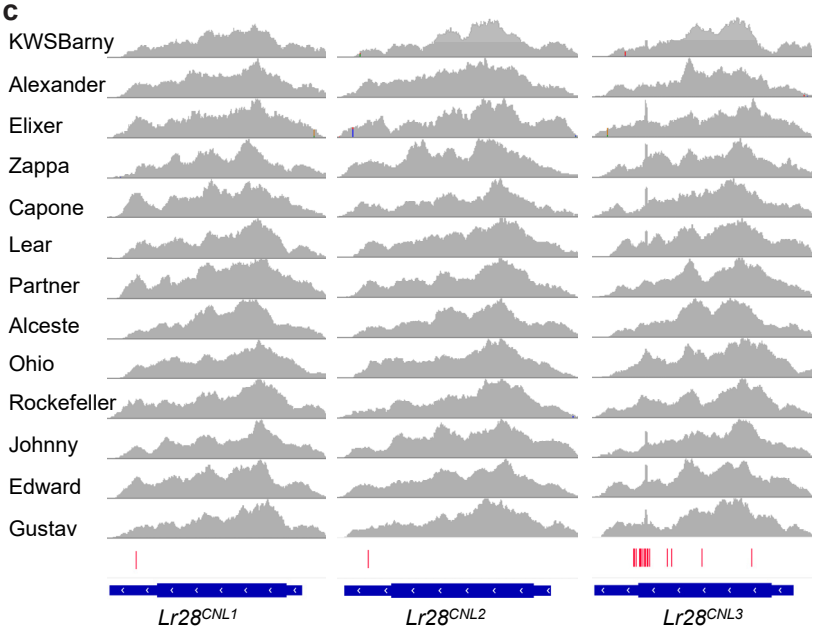
a



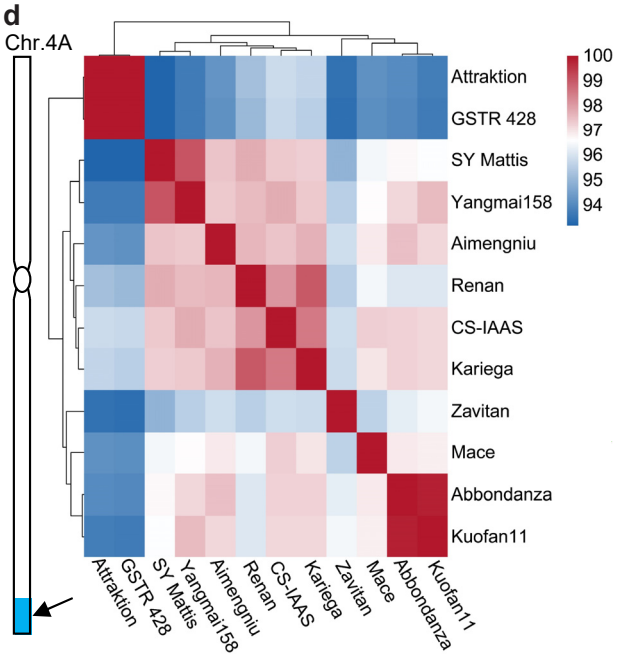
b

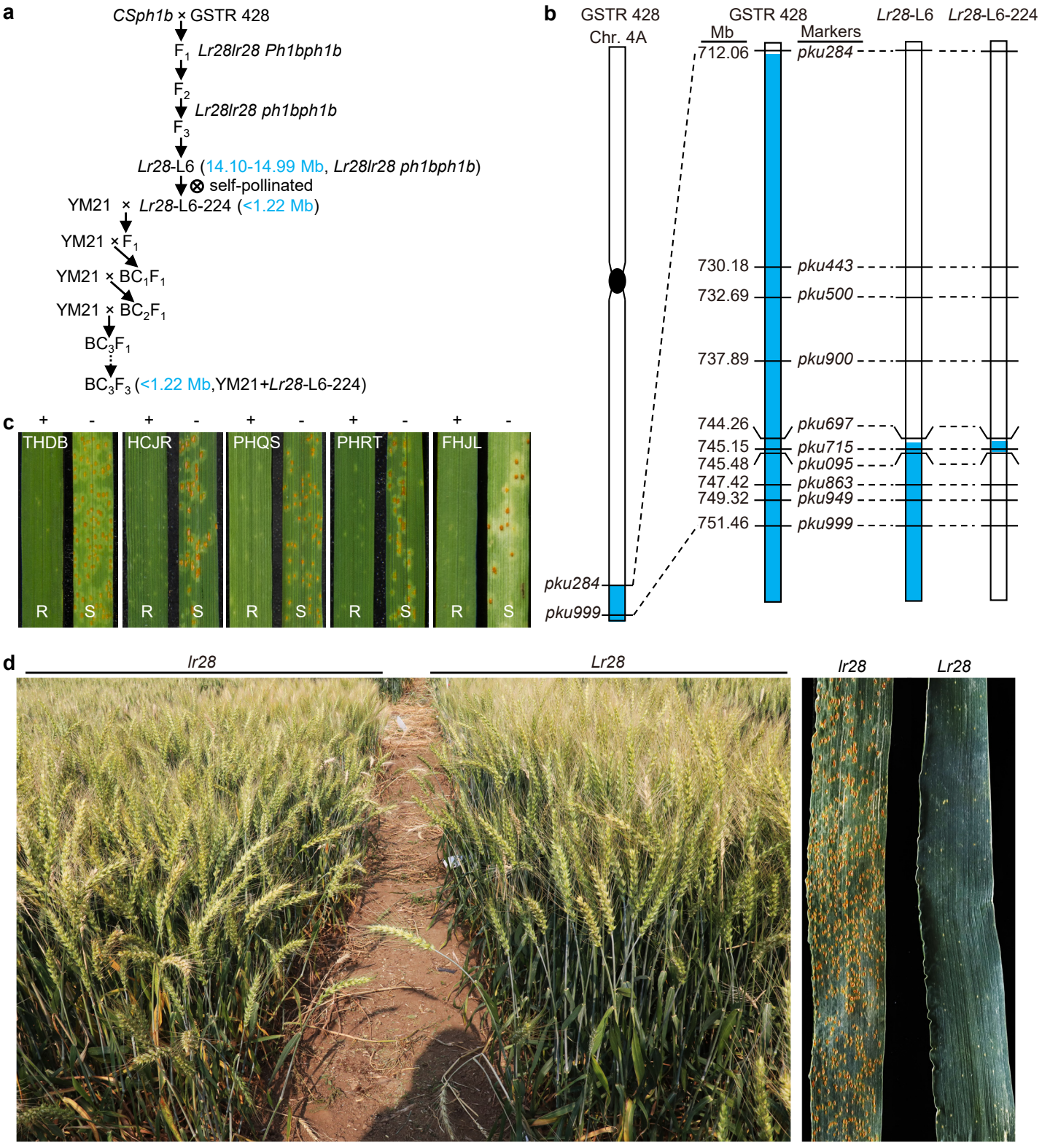
Position (aa)		100	193	646	652	851	859	932	976	1089	1107	1108	1137	1153	1164	1178	1182	1186	1217	1229	1233
$Lr28^{CNL1/CNL2}$	GSTR 428	R	L	Q	T	K	N	F	W	C	K	Y	R	T	R	S	W	A	R	I	T
$Lr28^{CNL3}$		R	F	Q	A	K	N	L	R	C	K	Y	G	A	K	E	W	G	I	V	R
$Lr28^{CNL1/CNL2}$	T2140003 T2140004	R	L	Q	T	K	N	F	W	C	K	Y	R	T	R	S	W	A	R	I	T
$Lr28^{CNL3}$	PI 369596 PI 542268	R	F	Q	A	K	N	L	R	C	K	Y	G	A	K	E	W	G	I	V	R
$Lr28^{CNL2}$	PI 369590 PI 369591 PI 369604	R	L	Q	T	K	N	F	W	C	K	Y	R	T	R	S	W	A	R	I	T
$Lr28^{CNL-hap3}$	PI 554295 PI 554297 PI 542266	R	L	R	A	K	N	F	R	C	K	Y	G	T	R	E	G	A	R	V	R
$Lr28^{CNL-hap4}$	PI 486263	R	L	R	A	T	N	F	R	C	K	Y	G	T	R	E	G	A	R	V	R
$Lr28^{CNL-hap5}$	PI 554303	C	L	R	A	K	N	F	R	C	K	Y	G	T	R	E	G	A	R	V	R
$Lr28^{CNL-hap6}$	PI 573450	R	F	Q	A	K	K	F	R	R	N	N	G	T	R	S	W	A	I	V	R
$Lr28^{CNL-hap7}$	PI 573452	R	L	Q	A	K	K	F	R	R	N	N	G	T	R	S	W	A	I	V	R

c



d




a
CSph1b × GSTR 428
F1 Lr28lr28 Ph1bph1b
F2
Lr28lr28 ph1bph1b
F3
Lr28-L6 (14.10-14.99 Mb, Lr28lr28 ph1bph1b)
⊗ self-pollinated
YM21 × Lr28-L6-224 (<1.22 Mb)
YM21 × F1
YM21 × BC1F1
YM21 × BC2F1
BC3F1
BC3F3 (<1.22 Mb,YM21+Lr28-L6-224)
b
GSTR 428
Chr. 4A
GSTR 428
Mb
Markers
Lr28-L6
Lr28-L6-224
712.06
pku284
730.18
pku443
732.69
pku500
737.89
pku900
744.26
pku697
745.15
pku715
745.48
pku095
747.42
pku863
749.32
pku949
751.46
pku999
pku284
pku999
c
+ - + - + - + - + -
THDB
HCJR
PHQS
PHRT
FHJL
R S R S R S R S R S
d
Ir28
Lr28
Ir28
Lr28

Supplementary Files

This is a list of supplementary files associated with this preprint. Click to download.

- SupplementaryTables113.xlsx
- SupplementaryFigs.122.pdf
- nrreportingsummaryLr28.pdf
- SupplementaryfileuncroppedGels.pdf